Calibration Report of the CIS Measurements in the Cluster Active Archive (CAA)

prepared by

I. Dandouras, A. Barthe, L. Kistler, A. Blagau

DOCUMENT STATUS SHEET

Issue	Date	Details
Version 1.0	30.01.2009	1st version, prepared for the CAA Peer Review. Document referenced as CAA-EST-CR-CIS.
Version 1.1	17.05.2010	Various updates, in preparation of the 5th CAA Operations Review.
Version 1.2	29.04.2011	Various updates, in preparation of the 6th CAA Operations Review.
Version 1.3	10.05.2012	Various updates, in preparation of the 7th CAA Operations Review.
Version 1.4	09.05.2013	Various updates, following the 2013 CIS-CAA Progress Meeting and in preparation of the 8th CAA Operations Review.
Version 1.5	12.05.2014	Various updates, in preparation of the 9th CAA Operations Review.
Version 1.6	29.10.2015	Various updates, in preparation of the 10th CAA Operations Review.
Version 1.7	15.05.2017	Various updates, in preparation of the 11th CAA Operations Review.
Version 2.0	24.02.2025	Various updates, following the end of the Cluster science instruments operations phase.

Table of Contents

1 Introduction

The Cluster Active Archive (CAA) / Cluster Science Archive (CSA)) aims at preserving the complete set of the measurements collected by the four Cluster spacecraft, properly calibrated, so that they are usable in the long-term by the world-wide scientific community as well as by the instrument team PIs and Co-Is (Perry et al., 2006; Escoubet et al., 2021).

The CIS (Cluster Ion Spectrometry) experiment, consisting of HIA and CODIF detectors, is a comprehensive ionic plasma spectrometry package onboard the four Cluster spacecraft, capable of obtaining full three-dimensional ion distributions (about 0 to 40 keV/e) with a time resolution of one spacecraft spin (4 sec) and with mass-per-charge composition determination (Rème et al., 2001).

The quality of the CIS data products archived at the CSA is based on the calibration files that include:

- parameters determined during ground calibrations in vacuum test facilities and are stable through the mission,
- parameters that change gradually through the mission,
- parameters that can be changed during the mission by command.

All of them are equally important in converting raw data into physical units, and are used together. The MCP (Microchannel Plate) particle detection efficiency degradation as a function of time is the single most important parameter to track and adjust during the mission. This includes total efficiency values, i.e. average response over the MCP surface, and anode cross-calibrations (relative efficiencies). Total efficiency evolution is evaluated by cross-calibrating the CIS provided densities with the density values provided by the Whisper sounder experiment (Décréau et al., 2001). In addition CODIF provides also the time-of-flight performance statistics, which give a measure of the total efficiency evolution. Anode cross-calibrations are performed in gyrotropic plasma regimes.

An overview of these calibration procedures and their results is given in the present document.

A guide for the user of the CIS data is given in the “User Guide to the CIS measurements in the Cluster Active Archive” (Dandouras and Barthe, 2025).

2 Instrument Description

The CIS package consists of two different instruments (Rème et al., 2001):

- a time-of-flight ion *Composition and Distribution Function* analyser (*CODIF*, or *CIS-1*),
- a *Hot Ion Analyser* (*HIA*, or *CIS-2*).

In addition, each of the instruments, in order to be able to cover a dynamic range of about 7 orders of magnitude in particle fluxes, provides two different geometric factors: a *high-sensitivity side* (or *HS*) and a *low-sensitivity side* (or *LS*).

2.1 The CODIF (CIS-1) Instrument

The CODIF instrument combines ion energy per charge selection, by deflection in a rotationally symmetric toroidal electrostatic analyser, with a subsequent time-of-flight analysis after post-acceleration to ~15 keV/e. Ions are selected as a function of their *E/q* (energy per charge) ratio, by sweeping the high voltage applied between the two toroidal hemispheres. The full energy sweep with 31 contiguous energy channels is performed 32 times per spin. In the time-of-flight (TOF) section the velocity of the incoming ions is measured, which allows then the calculation of their *m/q* (mass per charge) ratio. Microchannel Plate (MCP) electron multipliers are used to detect both the ions and the secondary electrons, which are emitted from a carbon foil at the entry of the TOF section, during the passage of the ions. These secondary electrons give the "start" signal, for the time-of-flight measurement, and the position information (elevation angle of the incoming ion, provided by the MCP sectoring in anodes), cf. Fig. 2.1.

In order to cover populations ranging from magnetosheath protons to tail lobe ions, a dynamic range of more than 10^5 is required. CODIF therefore consists of two sections, each with a 180° field of view, with geometry factors differing by a factor of ~ 100. This way, one of the sections will have counting rates which are statistically meaningful and which at the same time can be handled by the time-of-flight electronics. However, intense ion fluxes can in some cases saturate the CODIF instrument (particularly if data are acquired from the high sensitivity side), but these fluxes are measured with HIA. The operation of the high-sensitivity side ("high-G", or "HS") and of the low-sensitivity side ("low-g", or "LS") on CODIF is mutually exclusive, and only one of the two sides can be selected at a time to supply data.

With an additional Retarding Potential Analyser (RPA) device in the aperture system of the CODIF sensor, and with pre-acceleration for the energies below 25 eV/e, the range is extended to energies as low as the spacecraft potential. The retarding potential analyser operates only in the RPA mode,

and provides an energy range between about 0.7 and 25 eV/e (with respect to the spacecraft potential).

2.2 The HIA (CIS-2) Instrument

The HIA instrument is an ion energy-spectrometer, capable of obtaining full three-dimensional ion distributions with good angular and time resolution (one spacecraft spin). HIA combines the selection of incoming ions, according to the ion energy per charge by electrostatic deflection in a quadrispherical analyser, with a fast imaging particle detection system. This particle imaging is based on Microchannel Plate (MCP) electron multipliers and position encoding discrete anodes. As for CODIF, ions are selected as a function of their E/q (energy per charge) ratio, by sweeping the high voltage applied between the two hemispheres, cf. Fig. 2.2.

In order to cover populations ranging from solar wind and magnetosheath ions to tail lobe ions, a dynamic range of more than 10^5 is required. HIA therefore consists of two 180° field-of-view sections, with two different sensitivities (with a ~20 ratio), corresponding respectively to the high-sensitivity ("high-G", or "HS") and to the low-sensitivity ("low-g", or "LS") side. The "low g" side allows detection of the solar wind and the required high angular resolution is achieved through the use of 8 sectors (or MCP anodes), 5.625° each, the remaining 8 sectors having 11.25° resolution. The 180° "high G" side is divided into 16 sectors, 11.25° each. For each sensitivity side a full 4π steradian scan, consisting of 32 energy sweeps, is completed every spin of the spacecraft, i.e. every 4 s, giving a full three-dimensional distribution of ions in the energy range ~5 eV/e - 32 keV/e.

3 Measurement Calibration Procedures

3.1 Calibration files

Both CODIF and HIA have been very well calibrated before launch, in vacuum test facilities (Rème et al., 2001). However, due to the in-flight evolution of the MCP detection efficiencies as a function of time, the CIS calibration files are updated regularly. A calibrations catalogue file, which is provided with the calibration files, serves as a pointer to which calibration files to use for each data time period. This catalogue file evolves in an incremental way through the mission, to take into account the existence of new calibration files, which correspond to the instrument particle detection efficiency evolution, or other changes in the instrument.

Calibration files include thus:

- parameters that have been determined during ground calibrations in vacuum test facilities and are stable through the mission (e.g. instrument angle response, electrostatic analyser constant used in the calculation of the energy sweep tables, etc.),
- parameters that change gradually through the mission (e.g. particle detection efficiencies),
- parameters that can be changed during the mission by command (e.g. upload of new spin accumulation tables for 3-D ion distributions in the various modes).

All of them are equally important in converting raw data into physical units, and are used together. How the calibration values are used to convert particle raw counts in physical units, such as particle flux, or moments of the ion distribution functions, is described in Appendix A.

3.2 Detector efficiency

Detection efficiency degrades with time, due to the MCP gain fatigue mechanism (Prince and Cross, 1971). The physical degradation of the MCPs during the mission is in some extent compensated by applying increased high voltages on the MCP plates, to restore as much as possible secondary electron gain in the MCP channels albeit the physical degradation of their emissive surfaces. The procedure used onboard for testing the necessity for an eventual MCP HV increase in shown in Figure 3.1.

Updating the calibration files for the detection efficiency evolution, with respect to the pre-launch calibrations, is a multi-step process, and is performed a few times per year, or any time when the MCP voltage is changed.

3.2.1 Determination of HIA efficiency

For HIA the **detection efficiency** is given by:

$$\boldsymbol{Eff}\ (PF, E)^{-1} = Norm\_\Theta * Eff\ (E) * Cheff(\Theta) * [\ 1\ /\ T(E)]$$

where:

- E is the ion energy
- $Norm\_\ \Theta$ is an anode normalisation coefficient (one value for the HS and one for the LS side)
- $Eff\ (E)$ is an Energy-dependent efficiency term, given by $Eff\ (E) = A * E + B$ (A, B : linear coefficients, one for the HS and one for the LS side)
- $Cheff(\Theta)$ is an Anode - dependent efficiency coefficient
- $T(E)$ is an MCP energy-dependent efficiency, given by $T(E) = T_0 + T_1*(E+E_g) + T_2*(E+E_g)^2$ (E_g : MCP grid acceleration energy)

This results in 41 efficiency calibration coefficients per validity period per spacecraft (2 + 4 + 32 +3). These coefficients need to be determined for each validity period that is determined by the MCP aging and/or MCP voltage variations.

In addition, g_E is an energy-independent geometric factor (one for the HS side and one for the LS side.

During the in-flight calibration procedure the HIA ion density values are compared and cross-calibrated with the electron density values supplied by the Whisper sounder experiment (Décréau et al., 2001). This is performed in the magnetosheath for the HS side and in the solar wind for the LS side, i.e. in the plasma environment where each of the two sides has the optimum performance, and where the plasma energy spectrum is within the energy domain covered by the instrument. It should be noted also that the HIA anodes relative efficiencies are remarkably stable, i.e. the efficiency drift is very homogeneous between the anodes (11.25° or 5.625° sectors).

More details for the HIA in-flight calibration procedure are given in Blagau et al., 2014.

3.2.2 Determination of CODIF efficiency

For CODIF, and for each of the four main ion species detected (H^+, He^{++}, He^+, O^+), the **detection efficiency** is given by:

$$\boldsymbol{Eff}\,(PF, E, m) = (M_0 + M_1*E + M_2*E^2 + M_3*E^3\ ) * Abs\_Eff$$

where:

- M_0 ... M_3 are the efficiency calibration coefficients, depending on the ion species m (4 sets, for H^+, He^{++}, He^+, and O^+), and on the detection anode PF
- E is the total ion energy (ion energy + post-acceleration energy)
- Abs_Eff is the absolute efficiency (one value per ion species m for the HS and one for the LS side)

This results in 232 efficiency calibration coefficients per spacecraft (4 x 4 x 14) + (2 x 4). These coefficients need to be determined for each validity period that is determined by the MCP aging and/or MCP voltage variations.

In addition, g_E is an e energy-independent geometric factor (one for the HS side, one for the LS side and one for the RPA).

The CODIF calibrations updating is a more complex process. It involves the determination of the start-MCP efficiency, the stop-MCP efficiency, the fraction of coincidences between the “start” time-

of-flight signal and the "stop" time-of-flight signal that also have a "single position" signal, allowing thus to calculate the total efficiency. In addition, the efficiencies of the individual anodes (22.5° sectors) have to be cross-calibrated, since they slowly drift relative to each other, and this is performed by using time periods when the ion distributions are expected to be gyrotropic. CODIF calibrations involve also separate efficiencies determination for H^+ and O^+ ions.

Plasma pressure balance control, at the transition of plasma boundaries, is an additional tool for calibrating the CODIF efficiencies (Fig. 3.2).

The resulting CODIF H^+ measurements are also cross-checked with the HIA measurements, for periods when the plasma is composed mainly from H^+ ions, and with WHISPER, PEACE and WBD density data, when all these instruments are covering well the ambient plasma energy range. CODIF data are also cross-checked with the high-energy ion data supplied by the RAPID experiment (Wilken et al., 2001), for periods where energetic plasma is present in the energy range of both instruments (Kronberg et al., 2010).

The key issues during the CODIF in-flight calibrations are (see Fig. 3.3):

Overall Change in H^+ Efficiency:

- For Cluster spacecraft 4 use "monitor rate" data to track the start efficiency (SFR/SR: start/stop coincidence rate to stop rate), stop efficiency (SFR/SF) and the fraction of coincidences that also have a single position signal (SEV/SFR). The product of these values gives the total efficiency (cf. also Figs. 5.3 and 5.4).
- For Cluster 3 (for which the Stop rate, SR, does not work well) use comparison spectra with Cluster 4 for time periods when the two spacecraft are close.

Overall Change in O^+ Efficiency:

- Times are used when the count rate was dominated by O^+ (mainly times with O^+ "beams" in the lobe).
- Because after 2007 these do not give any more a sufficiently high-count rate, since then a comparison of O^+ spectra between Cluster 3 and Cluster 4 has been used.

- Analysis of long-term trends (over a solar cycle) of the O+/H+ ratio has been also performed, in 2013, which allowed a reassessment of the O^+ efficiency values after 2006 (cf. section 5.1.2).

Relative efficiency change between anodes for Cluster 3 and Cluster 4, H^+ and O^+:

- Use pitch angle spectra during gyrotropic time periods to normalise the different positions (anodes) within each instrument. This is done separately for H^+ and O^+.

More details for the CODIF in-flight calibration procedure given in Kistler et al., 2013.

4 Measurement Processing Procedures

The processing of the CODIF and HIA particle raw counts with calibration values, and their conversion into physical units, such as particle flux or moments of the ion distribution functions, is described in Appendix A ("CIS: Particle Counts to Flux and to Moments of the Ion Distribution Function").

The data processing requires three elements: CIS raw (L1) data, calibration files and the PI software. The processing is fully automated and produces output data files in CEF format.

5 Results of Calibration Activities

5.1 CODIF

For CODIF the efficiency degradation is pronounced, due to the operational principle of this instrument, requiring the detection of both the ion ("stop" time-of-flight signal) and of the electrons emitted by the carbon foil ("start" time-of-flight signal), plus a "position" signal, to validate the detection of an ion.

The physical degradation of the MCPs is in some extent compensated by applying increased high voltages on the MCP plates, to restore secondary electron gain in the MCP channels albeit the physical degradation of their emissive surfaces. Such MCP high voltage increases have been performed in July 2002, August 2002, July 2003, September 2004 (cf. also Fig. 5.3). The calibration files keep a detailed track of all these changes.

In 2008 the efficiencies for CODIF were reduced, on the average, to about 2% of the initial detection efficiencies on Cluster 4 (Fig. 5.1), and to less than about 5% on the "good" MCP quadrant on Cluster 3 (cf. CIS data caveats in Dandouras et al., 2010, and also the "User Guide to the CIS measurements in the Cluster Active Archive"). In spite of these low efficiency values, the CODIF

performance and ability to still collect data of quality adequate for addressing most of its scientific objectives has been remarkable.

In July 2009 the CODIF MCP high-voltage on Cluster spacecraft 4 was raised again by ~80 V, which increased the particle detection efficiency by a factor of ~2 and brought the efficiency back to the summer 2005 levels (Fig. 5.1). During the following 5 years the CODIF detection efficiency was remarkably stable. However, a slow efficiency decline tendency appeared again in 2015-2016 (Fig. 5.2). This later levelled-off, and during the last years of the mission the CODIF detection efficiency on Cluster 4 (the only CODIF operational instrument after 2009) was very stable.

The key limitations are:

- **Cluster 1**: The CODIF instrument has been switched off since 25 October 2004, due to an MCP high voltage anomaly.
- **Cluster 3:** The CIS experiment (CODIF and HIA) has been switched off since December 2009, due to a damaged electronic component in the instrument. In addition, before this, on the HS side only the upper quadrant of CODIF had adequate efficiency, resulting in a poor quality of moments (cf. the "User Guide to the CIS measurements in the Cluster Active Archive").
- **Cluster 4:** The CODIF instrument onboard this spacecraft has operated nominally throughout the mission.

5.1.1 H^+ efficiencies

CODIF calibration results, and efficiencies evolution for H^+ are given in Figures 5.1 and 5.2.

Figure 5.3 shows the evolution of each of the three signals, i.e. "stop" time-of-flight signal, "start" time-of-flight and "position" signal (cf. section 3.2.2) for Cluster 4, from the beginning of the mission until late 2012. A "zoom" for the period starting from September 2006, with an extension up to July 2015, is provided in Figure 5.4.

Figure 5.1 shows the total efficiency evolution for this spacecraft, separately for the HS and the LS. The efficiency improvement, resulting from the MCP high-voltage increase in July 2009, is clear in Figures 5.1 to 5.4.

The total H^+ efficiency evolution, for the three Cluster spacecraft, is shown in Figure 5.5.

5.1.2 O^+ efficiencies

Figure 5.6 shows the evolution of MCP efficiencies for O^+ on Cluster 1 and 4. Note that, for Cluster 4, the O^+ efficiency was revised in 2013, following the analysis of long-term trends (over a solar cycle) of the O^+/H^+ ratio. The H^+ efficiency is shown for comparison.

5.1.3 CODIF inter-anode comparisons

Figure 5.7 shows the comparison of inter-anode efficiencies for H^+ on Cluster 3 and Cluster 4. As discussed in section 3.2.2, pitch-angle distribution plots are used in areas where the plasma distribution is expected to be gyrotropic in order to adjust the inter-anode efficiencies.

5.2 HIA

The particle detection efficiency degradation is moderate for the HIA instrument. The physical degradation of the MCPs is in some extent compensated by applying increased high voltages on the MCP plates, to restore secondary electron gain in the MCP channels albeit the physical degradation of their emissive surfaces. These high voltage increases are shown in Figure 5.8. Since February 2007 there has been no other change in these MCP high voltages.

5.2.1 HIA inter-anode comparisons

The HIA relative anode response, in an isotropic plasma, is shown in Figure 5.9.

It should be also noted that the HIA anodes relative efficiencies are remarkably stable, i.e. the efficiency drift is very homogeneous between the anodes (11.25° or 5.625° sectors).

5.2.2 Variation of HIA efficiency

Figure 5.10 gives the evolution of the HIA HS and LS calibration factors for Cluster 1 (black) and Cluster 3 (red), following the high voltage increases on the MCP plates. Data here are plotted from the beginning of the mission until October 2015. Note that HIA onboard Cluster 3 did not operate after December 2009, and that HIA onboard Cluster 1 efficiencies since 2013 were relatively stable, due to the short operation intervals then (see below), that minimised any further MCP gain fatigue.

For comparison with CODIF cf. Figure 5.5.

The key limitations are:

- **Cluster 1**: The HIA HS was the only operational side of the instrument after April 2011. Since November 2012 the duration of operations was also limited to 1 hour per orbit, (and up to 2 x 1 hour per day since December 2016), becoming even shorter later, due to an issue related to the ageing of the analyser sweep high-voltage supply system. Since 5 February 2021, due to a

failure in an electronic component the instrument has been operating in PROM mode only, which provides a snapshot of raw part counts (uncalibrated data), cf. the CIS Users Guide (Dandouras and Barthe, 2025)

- **Cluster 3:** The CIS experiment (CODIF and HIA) has been switched off since December 2009, due to a damaged electronic component in the instrument.
- **Cluster 4:** The HIA instrument has been switched off since the beginning of the science operations (2001).

6 Results of Cross-Calibration Activities

As indicated in section 3, the HIA ion density values are compared and cross-calibrated with the electron density values supplied by the Whisper sounder experiment (Décréau et al., 2001). This is performed in the magnetosheath for the HS side and in the solar wind for the LS side, i.e. in the plasma environment where each of the two sides has the optimum performance, the plasma energy spectrum is within the energy domain covered by the instrument and spacecraft charging effects are negligible.

6.1 HIA efficiency

Figure 6.1 shows a typical example of HIA - Whisper density cross-calibration in the magnetosheath (HS side). It is from a May 2009 event, used in fine-tuning HIA calibrations. 2777 data points were used in this example, and the root-mean-square deviation of the HIA to Whisper calculated densities is here 3.7 %. Similar procedure is used in the solar wind, to fine-tune the LS side of HIA.

Figures 6.2 shows an example of density comparison between the HIA instrument and the Whisper experiment, in the magnetosheath (Cluster 1 and Cluster 3). The fit between the two density plots is excellent.

6.2 CODIF efficiency

Figure 6.3 shows the same example for CODIF onboard Cluster spacecraft 4, where the LS side is operating, which is the one suited for the magnetosheath. Notice that on spacecraft 4 the CODIF LS side is used in the magnetosheath, in order to have better ion moments, as HIA is off on this spacecraft. Again the fit between the two density plots can be very good.

However, there are cases where the two instruments do not give the same results. Section 6.2 of the CIS Users Guide (Dandouras and Barthe, 2025) discusses the conditions where such discrepancies can appear, and the related caveats. Section 6.1 of the CIS Users Guide provides a data selection guide, in order to help the user select the most appropriate of the two instruments, as a function of the plasma environment analysed.

Figure 6.4 shows a typical example for HIA and CODIF density values comparison with the WHISPER provided density in the cusp, where the spacecraft is going through a large dynamic range of density values. The negative of the spacecraft potential value, measured by the EFW experiment, is also given. In the relatively high-density plasma (> 2 cm^{-3}), where spacecraft charging effects are small, the fit between the two CIS instruments and the Whisper density measurements is very good. In the low density part, however, where spacecraft charging to a positive floating potential repels the low-energy ions, which cannot any more be detected by CIS, HIA and CODIF provide, as expected, underestimated density values.

Figure 6.5 shows a case of CODIF density values comparison with the PEACE provided density in the magnetotail plasma sheet. This is a case of a dense plasma sheet (> 1 cm^{-3}), where spacecraft charging is low, and the two experiments give very consistent density values. This is not however the case in more typical tenuous plasma sheet events (< 1 cm^{-3}), where spacecraft charging to a positive floating potential does not allow the detection by CIS of low-energy ions.

The CODIF ion flux values have been also controlled for consistency with the RAPID-IMS flux values, in the overlapping energy range of the two instruments (~29-40 keV/e). Since the energy bins of the two instruments do not exactly match each other, this involved a comparison by fitting kappa distribution functions through the energy spectra of the two instruments (Kronberg et al., 2010). Figure 6.6 provides an example of such a cross-calibrated ion energy spectrum in the plasma sheet.

6.3 HIA-CODIF Cross-Calibration

Figure 6.7 shows a comparison of orbit averages of the density and the three components of the velocity for CODIF on Cluster 4, and HIA on Cluster 1 and Cluster 3, in GSE coordinates. The *x* and *y* coordinates are approximately in the spin plane, and so the relative anode efficiency does not significantly affect these velocities. The *z* coordinate is almost along the spin axis, so any discrepancies in the relative anode efficiencies would be observed here. It is expected that the average velocity in *z* should be 0. The relative anode efficiencies are adjusted to keep the error to less than 15 km s^{-1} (Kistler et al., 2013).

7 Summary

In summary, the detection efficiency degradation throughout the mission has been moderate for HIA, more pronounced (but reasonable) for CODIF, due to the operational principle of this instrument. The calibration files, which are used in processing the CIS data that are then archived at the CSA, keep a detailed track of all these evolutions.

In spite of these efficiency degradations, the ability of the HIA and CODIF instruments to collect data of quality adequate for addressing most of the scientific objectives has been remarkable, as indicated also by the more than 1300 science papers published, based on the analysis of these data (cf. list of representative CIS publications at http://cluster.irap.omp.eu/publications/list).

8 References

Blagau, A., I. Dandouras, A. Barthe, S. Brunato, G. Facskó, V. Constantinescu: In-flight calibration of Hot Ion Analyser onboard Cluster, Geosci. Instrum. Method, 3, 49, doi:10.5194/gi-3-49-2014 (2014)

Dandouras, I., A. Barthe: User Guide to the CIS measurements in the Cluster Active Archive (CAA). CAA-EST-UG-CIS (2025)

Dandouras, I., A. Barthe, E. Penou, S. Brunato, H. Rème, L.M. Kistler, M.B. Bavassano-Cattaneo, A. Blagau, and the CIS Team: Cluster Ion Spectrometry (CIS) Data in the Cluster Active Archive (CAA). In: Proceedings of the Cluster Workshop and CAA School, Springer, p. 51-72, (2010)

Décréau ,P.M.E., P. Fergeau, V. Krasnoselskikh, E. Le Guirriec, M. Lévêque, Ph. Martin, O. Randriamboarison, J.L. Rauch, F.X. Sené, H.C. Séran, J.G. Trotignon, P. Canu, N. Cornilleau, H. de Féraudy, H. Alleyne, K. Yearby, P.B. Mögensen, G. Gustafsson, M. André, D.C. Gurnett, F. Darrouzet, J. Lemaire, C.C. Harvey, P. Travnicek: Early results from the Whisper instrument on Cluster: an overview. Ann. Geophys., **19**, 1241 (2001)

Escoubet, C. P., A. Masson, H. Laakso, M. L. Goldstein, T. Dimbylow, Y. V. Bogdanova, M. Hapgood, B. Sousa, D. Sieg, and M. G. G. T. Taylor: Cluster After 20 Years of Operations: Science Highlights and Technical Challenges. J. Geophys. Res., doi: 10.1029/2021JA029474 (2021)

Kistler, L. M., C. G. Mouikis, K. J. Genestreti: In-flight Calibration of the Cluster/CODIF sensor, Geosci. Instrum. Method, 2, 225-235, doi:10.5194/gi-2-225-2013 (2013)

Kronberg, E., P. Daly, I., Dandouras, S. Haaland: Generation and validation of ion energy spectra based on Cluster RAPID and CIS measurements. In: Proceeding of the Cluster Workshop and CAA School, Springer, p. 301-306 (2010)

Masson, A., et al.: Electron density estimation in the magnetotail: a multi-instrument approach. In: Proceedings of the Cluster Workshop and CAA School, Springer, (2010)

Perry, C., T. Eriksson, P. Escoubet, S. Esson, H. Laakso, S. McCaffrey, T. Sanderson, H. Bowen, A.Allen, C. Harvey: The ESA Cluster Active Archive. In: Proceeding of the Cluster and Double Star Symposium-5th Anniversary of Cluster in Space, ESA SP-598, Noordwjik (2006)

Prince, R.H., J.A. Cross: Gain Fatigue Mechanism in Channel Electron Multipliers. Rev. Sci. Instrum., **42**, 66; DOI:10.1063/1.1684879 (1971)

Rème, H., C. Aoustin, J.M. Bosqued, I. Dandouras, B. Lavraud, J.A. Sauvaud, A. Barthe, J. Bouyssou, Th. Camus, O. Coeur-Joly, A. Cros, J. Cuvilo, F. Ducay, Y. Garbarowitz, J.L. Medale, E. Penou, H. Perrier,

D. Romefort, J. Rouzaud, C. Vallat, D. Alcaydé, C. Jacquey, C. Mazelle, C. dâUston, E. Möbius, L.M. Kistler, K. Crocker, M. Granoff, C. Mouikis, M. Popecki, M. Vosbury, B. Klecker, D. Hovestadt, H. Kucharek, E. Kuenneth, G. Paschmann, M. Scholer, N. Sckopke, E. Seidenschwang, C.W. Carlson, D.W. Curtis, C. Ingraham, R.P. Lin, J.P. McFadden, G.K. Parks, T. Phan, V. Formisano, E. Amata, M.B. Bavassano-Cattaneo, P. Baldetti, R. Bruno, G. Chionchio, A. Di Lellis, M.F. Marcucci, G. Pallocchia, A. Korth, P.W. Daly, B. Graeve, H. Rosenbauer, V. Vasyliunas, M. McCarthy, M. Wilber, L. Eliasson, R. Lundin, S. Olsen, E.G. Shelley, S. Fuselier, A.G. Ghielmetti, W. Lennartsson, C.P. Escoubet, H. Balsiger, R. Friedel, J-B. Cao, R. A. Kovrazhkin, I. Papamastorakis, R. Pellat, J. Scudder, B. Sonnerup: First multispacecraft ion measurements in and near the Earth's magnetosphere with the identical Cluster ion spectrometry (CIS) experiment. Ann. Geophys., **19**, 1303 (2001)

Wilken, B., P.W. Daly, U. Mall, K. Aarsnes, D.N. Baker, R.D. Belian, J.B. Blake, H. Borg, J. Büchner, M. Carter, J.F. Fennell, R. Friedel, T.A. Fritz, F. Gliem, M. Grande, K. Kecskemety, G. Kettmann, A. Korth, S. Livi, S. McKenna-Lawlor, K. Mursula, B. Nikutowski, C.H. Perry, Z.Y. Pu, J. Roeder, G.D. Reeves, E.T. Sarris, I. Sandahl, F. Søraas, J. Woch, Q.-G. Zong: First results from the RAPID imaging energetic particle spectrometer on board Cluster. Ann. Geophys., **19**, 1355 (2001)

9 Appendix A: “CIS: Particle Counts to Flux and to Moments of the Ion Distribution Function” document

Version 4.0
November 2006

Centre d'Etude Spatiale des Rayonnements

CIS :

Particle Counts to Flux

and to Moments of the Ion Distribution Function

I. DANDOURAS for the CIS Team

0.0 REFERENCE DOCUMENTS

[1] *First multispacecraft ion measurements in and near the Earth's magnetosphere with the identical Cluster ion spectrometry (CIS) experiment,* H. Rème et al., Ann. Geophys., 19, 1303, 2001.

[2] *CIS Experiment: Level 1 Data File Structure,* A. Barthe, CESR, 2000.

[3] *CIS Data Processing: Calibration File Structure*, A. Barthe and I. Dandouras, CESR, 2002.

[4] *CODIF Calibration Report - Part I : Efficiency Calculation*, L. M. Kistler, UNH, 2000.

[5] *CIS-2 Instrument: Summary of Calibration Tables*, J.-M. Bosqued, CESR, 2000.

[6] *Handbook PC12*, Philips Components, 1991.

[7] *The Plasma Composition Spectrometer PROMICS-3 in the INTERBALL Project*, I. Sandahl et al., in *Interball: Mission and Payload*, p. 178, CNES-IKI-RKA, 1995.

[8] *Cluster CIS-1 Product Information*, C. A. Ingraham, SSL-UCB, 1998.

[9] *Cluster CIS-2 Instrument FM Normal Operation Software*, A.M. Di Lellis and V. Formisano, IFSI, 1995.

[10] *Description Syntaxique des Jeux de Données CIS*, I. Dandouras, CESR, 2000.

[11] *CIS 1 Solid Angle Tables*, C. A. Ingraham, SSL-UCB, 1996.

[12] *Measurement of Plasma Velocity Distributions*, in "Analysis Methods for Multi-Spacecraft Data", G. Paschmann and P.W. Daly, ISSI, 1998.

[13] *Performances of the CIS-2 (HIA) Instrument in the Solar Wind: Analysis and Suggested Improvements,* J.M. Bosqued, CESR, 1999.

[14] *Spectrométrie ionique dans la magnétosphère et le vent solaire. Simulation et précision des mesures coordonnées au moyen des 4 satellites de la mission Cluster.* C. Martz, PhD Thesis, Paul Sabatier University, Toulouse, 1993.

[15] *Moments of Plasma Velocity Distributions*, in "Analysis Methods for Multi-Spacecraft Data", G. Paschmann, A.N. Fazakerley and S.J. Schwartz, ISSI, 1998.

[16] *Active spacecraft potential control for Cluster - implementation and first results,* K. Torkar et al., Ann. Geophys., 19, 1289, 2001.

[17] *Coordinate Transformations for CIS,* I. Dandouras, CESR, 2002.

1 INTRODUCTION - SCOPE

The CIS (Cluster Ion Spectrometry) experiment onboard the 4 Cluster spacecraft [*Ref. 1*] is capable of obtaining full three-dimensional ion distributions with good time resolution (one spacecraft spin) and with mass-per-charge composition determination. The CIS package consists of two different instruments, the time-of-flight ion Composition Distribution Function Analyser (CODIF, or CIS-1), and the Hot Ion Analyser (HIA, or CIS-2): http://cluster.cesr.fr:8000/.

During the first level of data processing, the CIS data are organised in Level-1 files [*Ref. 2*]: decommutated, decompressed, and time-tagged data, organised in a time series of records. Each record has a header (same for all telemetry products), and then a data section, specific to each product. For 3D and 2D distributions, the data section is a set of particle counts, C, each one for a given solid angle and energy bin.

During Level-3 processing these particle counts data can be transformed :

1. First in "corrected counts", C_{cor_eff}, i.e. taking into account corrections to compensate for the ion detection efficiencies.
2. Then in (differential) particle flux F (or *flux*) (ions cm^{-2} s^{-1} sr^{-1} keV^{-1}).
3. Or in particle energy flux PEF (or F_E or J_E) (keV cm^{-2} s^{-1} sr^{-1} keV^{-1}).
4. Or in phase space density PSD (or *fdist* or f or VDF) (s^3 km^{-6}).

The necessary calibration data needed to perform this processing are in the CIS calibration files [*Ref. 3*]: 3DCO Calibration Files, unless otherwise stated.

2 CONVERSION TO CORRECTED COUNTS

If C is the "raw" number of counts (from the Level-1 files) and C_{cor_eff} is the "corrected" (for detection efficiency) number of counts, then:

$$C_{cor\_eff} = \frac{C}{Eff(E,\theta)} \qquad [2.1]$$

where the detection efficiency $Eff(E,\theta)$ ($Eff \leq 1$) is a function of the ion energy E, detection anode (giving the particle arrival direction elevation θ), ion species m (CODIF separates ion species, whereas HIA does not), time history of the detector, and flight model.

2.1 CODIF

For CODIF, and for each of the four main ion species detected (H^+, He^{++}, He^+, O^+), the detection efficiency is given by [*Ref. 4*] :

$$Eff(PF, E, m) = (M_0 + M_1*E + M_2*E^2 + M_3*E^3) * Abs\_Eff \qquad [2.2]$$

where :

- M_0 .. M_3 : efficiency calibration coefficients, depending on the ion mass m (4 sets, for H^+, He^{++}, He^+, and O^+), and on the detection anode PF (*PF1* … *PF8* for the high sensitivity HS side and *PF10* … *PF15* for the low sensitivity LS side, corresponding to the different particle arrival directions in elevation θ); values given in the `anode_effic_coeff_table` section of the calibration tables.

- E : total ion energy (ion energy + post-acceleration energy), in keV.

  Ion energy is given in the `anal_k_factor`, `energy_sweep_table_mag`, `energy_sweep_table_sw`, `energy_sweep_table_prom`, and `rpa_energy_table` sections of the calibration files, and the results are in eV (to be converted here in keV). In fact these tables give the E/q, where q is the ion charge in electron charge units ($q = 1$ except for He^{++} ions, where $q = 2$).

  Post acceleration is given by the Time-of-Flight post-acceleration voltage PAC (in V), in the `post_accel_volt` section of the calibration tables (to be converted here in kV), and the particle charge q.

  The total ion energy is thus given by $E = q * (E/q + PAC)$ [2.3]

- Abs_Eff : absolute efficiency (one value for the HS side and one value for the LS side), given in the ABSEFF Calibration Files. Abs_Eff keeps track of the overall efficiency evolution of the instrument, as a function of time, whereas the M_0 .. M_3 coefficients provide for the anode cross-calibrations, which also evolve as a function of time but in a much slower rate.

2.2 HIA

For HIA, the ion detection efficiency is given by [*Ref. 5*] :

$$Eff(PF, E)^{-1} = Norm\_\Theta * Eff(E) * Cheff(\Theta) * [\ 1 / T(E)\ ] \qquad [2.4]$$

where :

- *Norm_E* and *Norm_Θ* : Energy and anode normalisation coefficients (one value for the HS side and one value for the LS side), given in the `fitting_param` section of the calibration tables.
- *Eff(E)* : Energy-dependent efficiency term, given by the linear relationship:

  $Eff(E) = A * E + B$, where:

  A, *B* : linear coefficients, (one value for the HS side and one value for the LS side), given in the `fitting_param` section of the calibration tables.

  E : ion energy, in eV, is given in the `anal_k_factor`, `energy_sweep_table`, and `energy_sweep_table_prom` sections of the calibration files.
- *Cheff(Θ)* : Anode - dependent efficiency coefficients, given in the `anode_effic_table` section of the calibration tables (`theta_efficiency` column).
- *T(E)* : MCP energy-dependent efficiency, given by [*Ref. 6, 7*] :

  $$T(E) = T_0 + T_1*(E+E_g) + T_2*(E+E_g)^2 \quad \text{for} \quad E_{j-1} < (E+E_g) < E_j \qquad [2.5]$$

  where E and E_g are respectively the ion energy and the acceleration energy due to the MCP bias voltage (both in eV). The T coefficients, E_g and the energy domain boundaries E_j are given in the `MCP_fitting_param` section of the calibration tables.

3 CORRECTION FOR DEAD TIME

The corrected (for detection efficiency) number of counts, C_{cor_eff}, can be further corrected for the instrument dead time effects [e.g. *Ref. 12*].

The simplified formula for dead time correction (which for more accuracy should also take into account the sum of counts accumulated on the previous energy steps, and both the MCP dead-time and the amplifier dead-time effects, *Ref.* [13]), is :

$$C_{cor} = \frac{C_{cor\_eff}}{1 - \frac{\tau}{\Delta t}.C_{cor\_eff}} \qquad [3.1]$$

where :

- C_{cor} is the corrected (for dead time and for detection efficiency) number of counts.
- τ is the instrument dead time, given in the `dead_times` section of the calibration tables.
- Δt is the particle accumulation time (cf. section 4, but here limited to one spin).

For CODIF the situation is more complex, due to the combined effect of the start-MCP dead time, the stop-MCP dead time, and, most important, the dead time of the time-of-flight unit: once an ion has triggered a "start" signal, no more ion can be detected until a "stop" signal is detected, within a valid time-of-flight window. Correction for dead time effects is thus not possible without modelling the instrument response, and saturation effects are expected on the data, in the presence of high ion fluxes.

4 CONVERSION TO PARTICLE FLUX

The relationship between the corrected number of counts C_{cor} and the (differential) particle flux F is given by:

$$F\ (\mathrm{cm^{-2}\ s^{-1}\ sr^{-1}\ keV^{-1}}) = \frac{C_{cor}}{G\ (\mathrm{cm^2\ sr}) \cdot \Delta t\ (\mathrm{s}) \cdot \Delta E\ (\mathrm{keV})} \qquad [4.1]$$

or:

$$F\ (\mathrm{cm^{-2}\ s^{-1}\ sr^{-1}\ keV^{-1}}) = \frac{C_{cor}}{G\ (\mathrm{cm^2\ sr}) \cdot \Delta t\ (\mathrm{s}) \cdot E(\mathrm{keV}) \cdot \Delta E / E\ (\mathrm{keV/keV})}$$

or:

$$F\ (\mathrm{cm^{-2}\ s^{-1}\ sr^{-1}\ keV^{-1}}) = \frac{C_{cor}}{g_E\ (\mathrm{cm^2\ sr\ keV/keV}) \cdot \Delta t\ (\mathrm{s}) \cdot E(\mathrm{keV})} \qquad [4.2]$$

where:

- G : geometric factor (for the given anode), in $\mathrm{cm^2}$ sr. If the data product is summed over several anodes, then G is the sum of the geometric factors of the corresponding anodes.
- g_E : energy-independent geometric factor (for the given anode), in $\mathrm{cm^2}$ sr keV $\mathrm{keV^{-1}}$. It includes the instrument energy resolution $\Delta E/E$. If the data product is summed over several anodes, then g_E is the sum of the geometric factors of the corresponding anodes. g_E is given in the `geom_factor` section of the calibration tables. Note that $\Delta E/E$ is a constant for an electrostatic analyser (independent of energy).
- E : average ion energy (in keV) of the energy steps for the given data counter. Values calculated from the energy tables in the calibration files (results to be converted in keV from eV). The data counter actually includes ions detected in the [E-ΔE/2, E+ΔE/2] energy bin.
- Δt : accumulation time, given by

  $$\Delta t\ (\mathrm{s}) = \frac{N_{spins} * P_{spin}(\mathrm{s})}{N_\phi * N_E} \qquad [4.3]$$

  where :

  N_{spins} is the number of spins over which the data product was accumulated, and is given in the `accumulation_spin_table` section of the calibration tables.

  P_{spin} is the spin period (in sec.), and is given (in msec) in the data record headers of the Level 1 files [*Ref. 2*].

  N_ϕ is the number of azimuths (Energy sweeps) per spin, for the data product. The value of N_ϕ is specific to each data product [*Ref. 8, 9, 10*]. For solid angles near the polar directions (elevation $|\theta| > 45°$, depending on the data product), where adjacent solid angles might have been binned together [*Ref. 11*] :

For CODIF:

The counts of the adjacent solid angles have just been summed together [*Ref. 8*]. For these polar directions N_ϕ must thus be divided by the number of elementary solid angles binned together.

For HIA:

Initially the counts of the adjacent solid angles have been averaged onboard [*Ref. 9*]. N_ϕ , in this case, remains unchanged with respect to the non-binned solid angles of the same data product.

On the 24 April 2001 (DOY 114) a modification has been performed on the onboard software, and starting from this day the adjacent polar solid angles are summed together, in the 3D-88 angle TM products. For these TM products and for these polar directions N_ϕ must thus be divided by the number of elementary solid angles binned together. This modification is effective from:

s/c # 1 : Year 2001 DOY 114 10:40 UT

s/c # 3 : Year 2001 DOY 114 14:30 UT

N_E is the number of energy steps per sweep, for the data product, including "dead" steps (i.e. those used for the electrostatic analyser high voltage flyback). The following table thus applies:

Number of energy steps in the data product	N_E
62	64
31	32
16	16 [32 for the lowest energy step E_{15}, E_0 being the highest energy step]
8	8 [8×(4/3) for the lowest energy step E_7, E_0 being the highest energy step]

5 CONVERSION TO PARTICLE ENERGY FLUX

The relationship between the corrected number of counts C_{cor} and the particle energy flux F_E is given by:

$$F_E \text{ (keV cm}^{-2}\text{ s}^{-1}\text{ sr}^{-1}\text{ keV}^{-1}) = \frac{C_{cor} \cdot E \text{ (keV)}}{G \text{ (cm}^2\text{ sr)} \cdot \Delta t \text{ (s)} \cdot \Delta E \text{ (keV)}} \qquad [5.1]$$

or:

$$F_E \text{ (keV cm}^{-2}\text{ s}^{-1}\text{ sr}^{-1}\text{ keV}^{-1}) = \frac{C_{cor} \cdot E(\text{keV})}{g_E \text{ (cm}^2\text{ sr keV/keV)} \cdot \Delta t \text{ (s)} \cdot E(\text{keV})}$$

or:

$$F_E \text{ (keV cm}^{-2}\text{ s}^{-1}\text{ sr}^{-1}\text{ keV}^{-1}) = \frac{C_{cor}}{g_E \text{ (cm}^2\text{ sr keV/keV)} \cdot \Delta t \text{ (s)}} \qquad [5.2]$$

Particle energy flux is thus directly proportional to the (corrected) counting rate.

6 CONVERSION TO PHASE SPACE DENSITY

The relationship between the corrected number of counts C_{cor} and the distribution function phase space density *fdist* (also called velocity distribution function) is given by [e.g. *Ref. 14*]:

$$fdist = \frac{C_{cor}}{g_v \cdot v^4 \cdot \Delta t} \qquad [6.1]$$

where :

v (or v_i) : average particle velocity for the given energy bin E_i ; since $E_i = \frac{1}{2} m\ v_i^2 \ \rightarrow$ $v_i^2 = 2E_i / m$, m being the ion mass.

g_v : velocity geometric factor (for the given anode). It includes the instrument velocity resolution $\Delta v/v$. Since $E \propto v^2 \ \rightarrow \ \Delta E/E = 2\ \Delta v/v \ \rightarrow$

$$g_E = 2\ g_v \qquad [6.2]$$

Equation [6.1] thus becomes :

$$fdist = \frac{C_{cor}}{0.5 g_E \cdot \frac{4E_i^2}{m^2} \cdot \Delta t} = \frac{C_{cor} \cdot m^2}{2 g_E \cdot E_i^2 \cdot \Delta t} \qquad [6.3]$$

Given [5.2], [6.3] becomes:

$$fdist = F_E \cdot \frac{m^2}{2E_i^2} \qquad [6.4]$$

or:

$$fdist\ (\mathrm{s^3\ km^{-6}}) = F_E\ (\mathrm{keV\ cm^{-2}\ s^{-1}\ sr^{-1}\ keV^{-1}})\ \frac{(N_m \cdot 1.6726 \cdot 10^{-27}(\mathrm{kg}))^2}{2(E_i(\mathrm{eV}) \cdot 1.6022 \cdot 10^{-19}(\mathrm{J/eV}))^2} \cdot 10^{22}\ (\mathrm{cm^2/m^2\ m^6/km^6}) \qquad [6.5]$$

N_m being the ion atomic mass number (1 for protons).

7 MOMENTS CALCULATION

7.1 Density

Ion density n is the zero-order moment of the 3D ion distribution function [e.g. *Ref. 15*], given by:

$n = \iiint fdist(v)\ d^3v$, v : ion velocity

From [6.1], and taking into account the finite angular and velocity resolution of the instrument, this becomes:

$$n = \sum_i \frac{\Delta v_i}{g_v \cdot v_i^4} \sum_j v_i \cdot \Delta\phi_j \sum_k \cos\theta_k \cdot v_i \cdot \Delta\theta_k \frac{C_{cor}}{\Delta t}$$

or in practice, and considering equally sized angular bins:

$$n = \frac{\Delta\phi \cdot \Delta\theta}{g_v} \cdot \sum_i \frac{\Delta v_i}{v_i^2} \sum_j \sum_k \cos\theta_k \cdot \frac{C_{cor}}{\Delta t} \qquad [7.1]$$

or, from [6.2] :

$$n\ (\mathrm{cm}^{-3}) = \frac{\Delta\phi(\mathrm{rad})\cdot\Delta\theta(\mathrm{rad})}{0.5 g_E(\mathrm{cm}^2\,\mathrm{sr\ keV/keV})}\cdot\sum_i\frac{\Delta v_i}{v_i^{\,2}}\frac{1}{(\mathrm{cm/s})}\sum_j\sum_k\cos\theta_k\cdot\frac{C_{cor}}{\Delta t(\mathrm{s})} \qquad [7.2]$$

where:

$\Delta\phi$ and $\Delta\theta$: azimuth and elevation size (in rad) of each elementary solid angle in the phase space, corresponding to the C_{cor} measurement.

θ_k : average elevation of detection anode *k*.

j : azimuth index.

v_i : average particle velocity (in cm/s) for energy bin *i* :

$$E_i = \frac{1}{2} m\, v_i^2 \ \rightarrow\ v_i = \sqrt{\frac{2E_i}{m}}\ , \text{ or}$$

$$v_i\ (\mathrm{cm/s}) = \sqrt{\frac{2E_i(\mathrm{eV})\cdot 1.6022\cdot 10^{-19}(\mathrm{J/eV})}{N_m\cdot 1.6726\cdot 10^{-27}(\mathrm{kg})}}\ \text{x 100 cm/m}$$

Δv_i : size in phase space (in cm/s) for particles detected in energy bin *i* ($\Delta v_i = v_{max\,i} - v_{min\,i}$).

Note 1 : Density calculation results are sensitive to the accuracy of g_E and to the accuracy of corrections for detection efficiencies. They are also sensitive to eventual detector saturation in the presence of high ion fluxes (dead time effects).

Note 2 : The density calculated here in reality is the ion partial density in the energy domain covered by the instrument, typically 25 eV/q to 40 keV/q for CODIF and 5 eV/q to 32 keV/q for HIA. In the presence of cold plasma at energies below the instrument energy threshold, or of hot plasma at energies above the instrument upper energy limit, this partial density evidently is lower than the total plasma density.

Note 3 : The instrument energy domain is always defined with respect to the spacecraft potential. Spacecraft charging to a positive floating potential, as can be the case in low density plasmas when the ASPOC ion emitter for spacecraft potential control is not operating, repels the low-energy ions which in these cases cannot be detected by CIS [*Ref. 1*, *16*]. This effect results in a further increase of the difference between the partial density, measured by CIS, and the total density.

Note 4 : Eventual instrument background counts due to penetrating particles, from the radiation belts around perigee passes or during SEP (Solar Energetic Particles) events, can result in an overestimation of the density calculated here.

Note 5 : The entire velocity phase space, corresponding to the instrument energy domain, is not covered during all modes. This can be the case during solar wind modes, and some magnetosheath modes, where the summations in equations [7.1] and [7.2] are limited by the instrument operation to a subset of the phase space, in velocity and in solid angle coverage [cf. *Ref. 1* and http://cluster.cesr.fr:8000/ - link to "Caveats"].

7.2 Velocity

Ion bulk velocity vector $\underline{V}$ is the first order moment of the 3D ion distribution function, given by:

$$\underline{V} = \frac{1}{n} \iiint \underline{v}\, fdist(v)\, d^3v$$

or in practice:

$$V_x = \frac{1}{n} \frac{\Delta\phi \cdot \Delta\theta}{g_v} \cdot \sum_i \frac{\Delta v_i}{v_i} \sum_j \cos\phi_j \sum_k \cos^2\theta_k \cdot \frac{C_{cor}}{\Delta t}$$

$$V_y = \frac{1}{n} \frac{\Delta\phi \cdot \Delta\theta}{g_v} \cdot \sum_i \frac{\Delta v_i}{v_i} \sum_j \sin\phi_j \sum_k \cos^2\theta_k \cdot \frac{C_{cor}}{\Delta t}$$

$$V_z = \frac{1}{n} \frac{\Delta\phi \cdot \Delta\theta}{g_v} \cdot \sum_i \frac{\Delta v_i}{v_i} \sum_j \sum_k \sin\theta_k \cdot \cos\theta_k \cdot \frac{C_{cor}}{\Delta t} \qquad [7.3]$$

which gives :

$$V_x\,(\mathrm{cm/s}) = \frac{1}{n(\mathrm{cm}^{-3})} \frac{\Delta\phi(\mathrm{rad}) \cdot \Delta\theta(\mathrm{rad})}{0.5 g_E(\mathrm{cm}^2\mathrm{sr\ kev/keV})} \cdot \sum_i \frac{\Delta v_i}{v_i} \sum_j \cos\phi_j \sum_k \cos^2\theta_k \cdot \frac{C_{cor}}{\Delta t(\mathrm{s})}$$

$$V_y\,(\mathrm{cm/s}) = \ldots,\ V_z\,(\mathrm{cm/s}) = \ldots \qquad [7.4]$$

Note 1 : The plasma bulk velocity components in eq. [7.3] and [7.4] are given in the same reference frame as the 3D ion distribution function: the instrument-build system in the CIS Level-1 data files, or in pseudo-GSE in the CIS Level-3 data files delivered for archival to the

CAA (http://caa.estec.esa.int/caa/): X sunward, Z is the spacecraft axis and northward pointing. A coordinate transformation is then necessary to transform these vector components to the GSE system [*Ref. 17*], or to any other system.

Note 2 : Bulk velocity results are independent of the accuracy of g_E, and of the accuracy of the absolute efficiency values, due to the division by n (which includes 1/ g_E, and cancels g_E from the denominator in equation [7.4]). Results error bars, however, are sensitive to counting statistics.

Note 3 : The V_z term is very sensitive to the anode cross-calibrations, and in particular to those of the anodes looking in directions away from the spacecraft spin plane (high absolute values of $\sin\theta_k$: polar anodes). In some cases the efficiency calibration coefficients cannot completely compensate for strongly asymmetrically decreased efficiencies of such polar anodes, which results in a residual offset of V_z (e.g. case of CODIF onboard Cluster-sc3).

Note 4 : The spacecraft orbital velocity $\underline{v_{sc}}$ has here been assumed to be negligible. For more accurate calculations, however, velocity composition between $\underline{V}$ and $\underline{v_{sc}}$ might have to be considered.

7.3 Pressure

Ion pressure tensor P is the second order moment of the 3D ion distribution function, given (in the plasma centre of mass reference frame) by :

$$P = m \iiint (\underline{v}\text{-}\underline{V}) \cdot (\underline{v}\text{-}\underline{V})\, fdist(v)\, d^3v \qquad [7.5]$$

or

$$P = m\,[M - n\, \underline{V}\cdot\underline{V}] \qquad [7.6]$$

where M is the tensor in the measurement reference frame:

$$M = \iiint \underline{v}\cdot\underline{v}\, fdist(v)\, d^3v \qquad [7.7]$$

In practice:

$$M_{xx} = \frac{\Delta\phi \cdot \Delta\theta}{g_v} \cdot \sum_i \Delta v_i \sum_j \cos^2\phi_j \sum_k \cos^3\theta_k \cdot \frac{C_{cor}}{\Delta t}$$

$$M_{yy} = \frac{\Delta\phi \cdot \Delta\theta}{g_v} \cdot \sum_i \Delta v_i \sum_j \sin^2\phi_j \sum_k \cos^3\theta_k \cdot \frac{C_{cor}}{\Delta t}$$

$$M_{zz} = \frac{\Delta\phi \cdot \Delta\theta}{g_v} \cdot \sum_i \Delta v_i \sum_j \sum_k \sin^2\theta_k \cos\theta_k \cdot \frac{C_{cor}}{\Delta t}$$

$$M_{xy} = \frac{\Delta\phi \cdot \Delta\theta}{g_v} \cdot \sum_i \Delta v_i \sum_j \sin\phi_j \cos\phi_j \sum_k \cos^3\theta_k \cdot \frac{C_{cor}}{\Delta t}$$

$$M_{yz} = \frac{\Delta\phi \cdot \Delta\theta}{g_v} \cdot \sum_i \Delta v_i \sum_j \sin\ \phi_j \sum_k \sin\theta_k \cos^2\theta_k \cdot \frac{C_{cor}}{\Delta t}$$

$$M_{xz} = \frac{\Delta\phi \cdot \Delta\theta}{g_v} \cdot \sum_i \Delta v_i \sum_j \cos\phi_j \sum_k \sin\theta_k \cos^2\theta_k \cdot \frac{C_{cor}}{\Delta t} \qquad [7.8]$$

From [7.6] and [7.8] the pressure tensor elements, in the plasma centre of mass reference frame, are:

$$P_{xx} = m \cdot \left[\frac{\Delta\phi \cdot \Delta\theta}{g_v} \cdot \sum_i \Delta v_i \sum_j \cos^2\phi_j \sum_k \cos^3\theta_k \cdot \frac{C_{cor}}{\Delta t} - n \cdot V_x \cdot V_x \right]$$

$$P_{yy} = \ldots \qquad [7.9]$$

which gives :

$$P_{xx}\,(\text{nPa}) = N_m \cdot 1.6726 \cdot 10^{-24}\,(\text{g}) \cdot$$

$$\left[\frac{\Delta\phi(\text{rad}) \cdot \Delta\theta(\text{rad})}{0.5 g_E(\text{cm}^2\text{sr kev/keV})} \cdot \sum_i \Delta v_i(\text{cm/s}) \sum_j \cos^2\phi_j \sum_k \cos^3\theta_k \cdot \frac{C_{cor}}{\Delta t(\text{s})} - n\ (\text{cm}^{-3}) \cdot V_x \cdot V_x\ (\text{cm/s})^2 \right] \cdot$$

10^8 (nPa/(dyn cm^{-2}))

$$P_{yy}\,(\text{nPa}) = \ldots \qquad [7.10]$$

The pressure tensor

$$\mathbf{P} = \begin{matrix} P_{xx} & P_{xy} & P_{xz} \\ P_{yx} & P_{yy} & P_{yz} \\ P_{zx} & P_{zy} & P_{zz} \end{matrix}$$

can then be diagonalised, which for gyrotropic plasmas (distributions isotropic in the planes perpendicular to the magnetic field direction) gives:

$$P' = \begin{matrix} P_{xx}' & 0 & 0 \\ 0 & P_{yy}' & 0 \\ 0 & 0 & P_{zz}' \end{matrix} \qquad [7.11]$$

For non gyrotropic plasmas there are non-zero off-diagonal terms in [7.11], which can indicate the presence of shear stresses in the plasma.

Note 1 : Non-zero off-diagonal terms can also result from anode cross-calibration effects (cf. note on Vz, in section 7.2).

Note 2 : Alternatively, the P' tensor can be obtained from the P tensor not by diagonalising it, but by performing a rotation operation from the initial reference system (instrument-build or pseudo-GSE, cf. note in section 7.2) to a system where its *Z* axis is aligned to the magnetic field direction.

7.4 Temperature

The temperature tensor T (or T') is obtained from the pressure tensor P (or P') from the equation of state:

$$P' = n \cdot k \cdot T' \qquad [7.12]$$

where k is the Boltzmann's constant: $k = 1.380622 \times 10^{-23}$ J K^{-1}.

For each of the components of the temperature tensor we thus have:

$$T_{xx}'\,(\mathrm{K}) = \frac{P'_{xx}(\mathrm{Pa})}{n(\mathrm{m^{-3}})\cdot k} \rightarrow T_{xx}'\,(\mathrm{MK}) = \frac{P'_{xx}(\mathrm{nPa})\cdot 10^{-9}(Pa/nPa)\cdot 10^{-6}(\mathrm{MK/K})}{n(\mathrm{cm^{-3}})\cdot 10^{6}(\mathrm{cm^3/m^3})\cdot 1.380622\times 10^{-23}(\mathrm{J/K})} \rightarrow$$

$$T_{xx}'\,(\mathrm{MK}) = \frac{P'_{xx}(\mathrm{nPa})\cdot 10^{2}}{n(\mathrm{cm^{-3}})\cdot 1.380622}\,, \qquad T_{yy}'\,(\mathrm{MK}) = \ldots \qquad [7.13]$$

One can then define a scalar temperature :

$$T = \frac{T_{xx}'+T_{yy}'+T_{zz}'}{3} \qquad [7.14]$$

and a parallel T_{par} and perpendicular T_{perp} to the magnetic field temperature :

$$T_{par} = T'_{zz}, \qquad T_{perp} = \frac{T_{xx}'+T_{yy}'}{2} \qquad [7.15]$$

assuming the Z axis of the T' (or P') tensor corresponds to the magnetic field direction.

Expressing the temperature not in temperature units (K or MK) but in energy units (eV) actually gives the average ion energy in the distribution :

$$T\,(\text{eV}) = T\,(\text{K}) \cdot \frac{1.380622 \times 10^{-23}\,(\text{J/K})}{1.6022 \cdot 10^{-19}\,(\text{J/eV})} \cdot \frac{3}{2} \;\rightarrow\; T\,(\text{eV}) = 1.2925559 \text{ x } 10^{-4} \cdot T\,(\text{K})$$

or $T\,(\text{eV}) = 1.2925559 \text{ x } 10^{2} \cdot T\,(\text{MK})$ [7.16]

The factor 3/2 corresponds to the $1/2\,k\,T$ average particle energy per degree of freedom, multiplied by the three degrees of freedom for the movement of each particle in the 3D space.

Figures

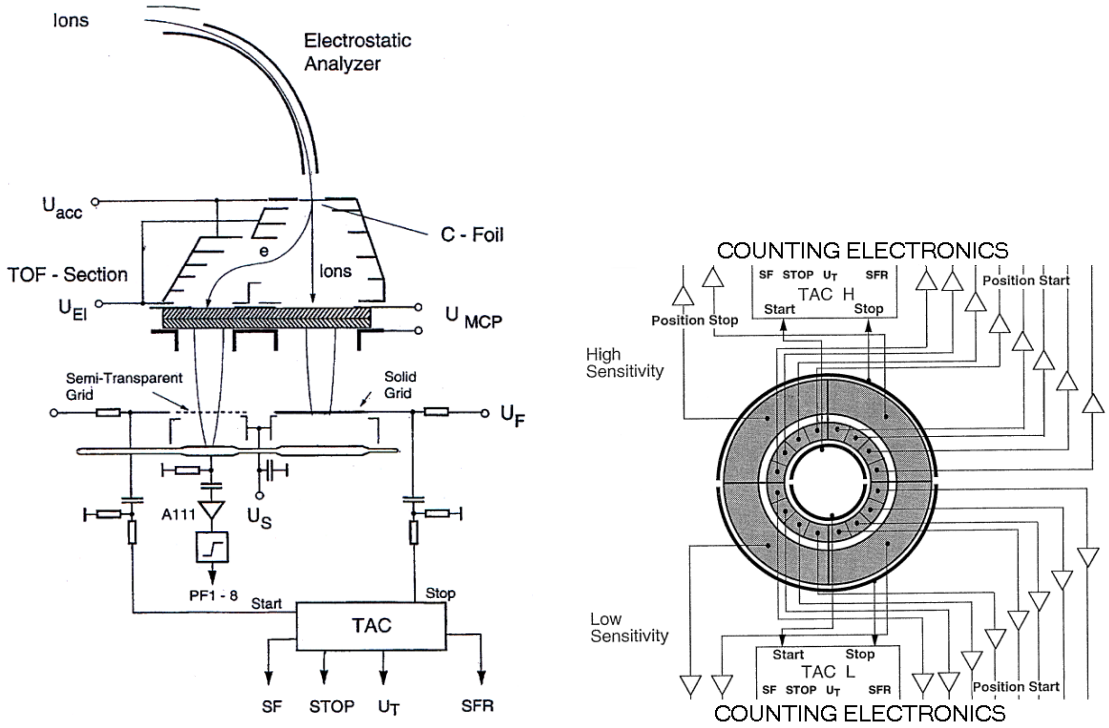

Figure 2.1

Schematic of the CODIF time-of-flight section (left) and MCP sectoring (right).

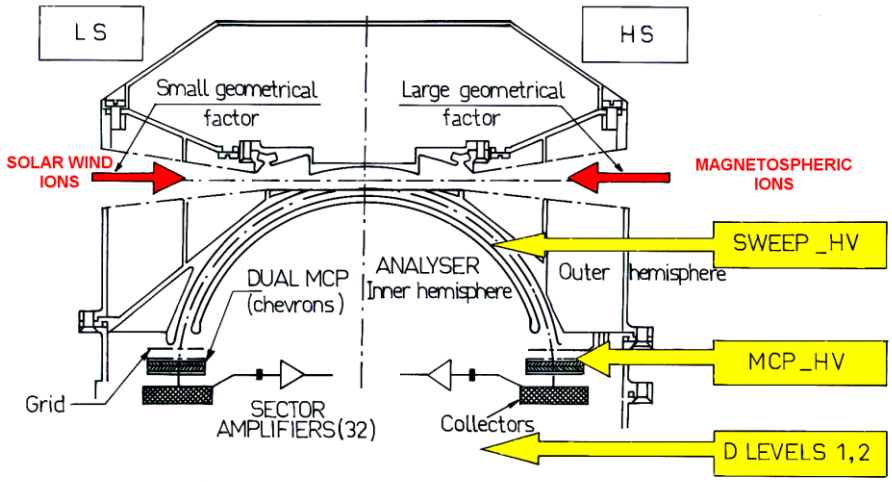

Figure 2.2

Cross sectional view of the HIA instrument.

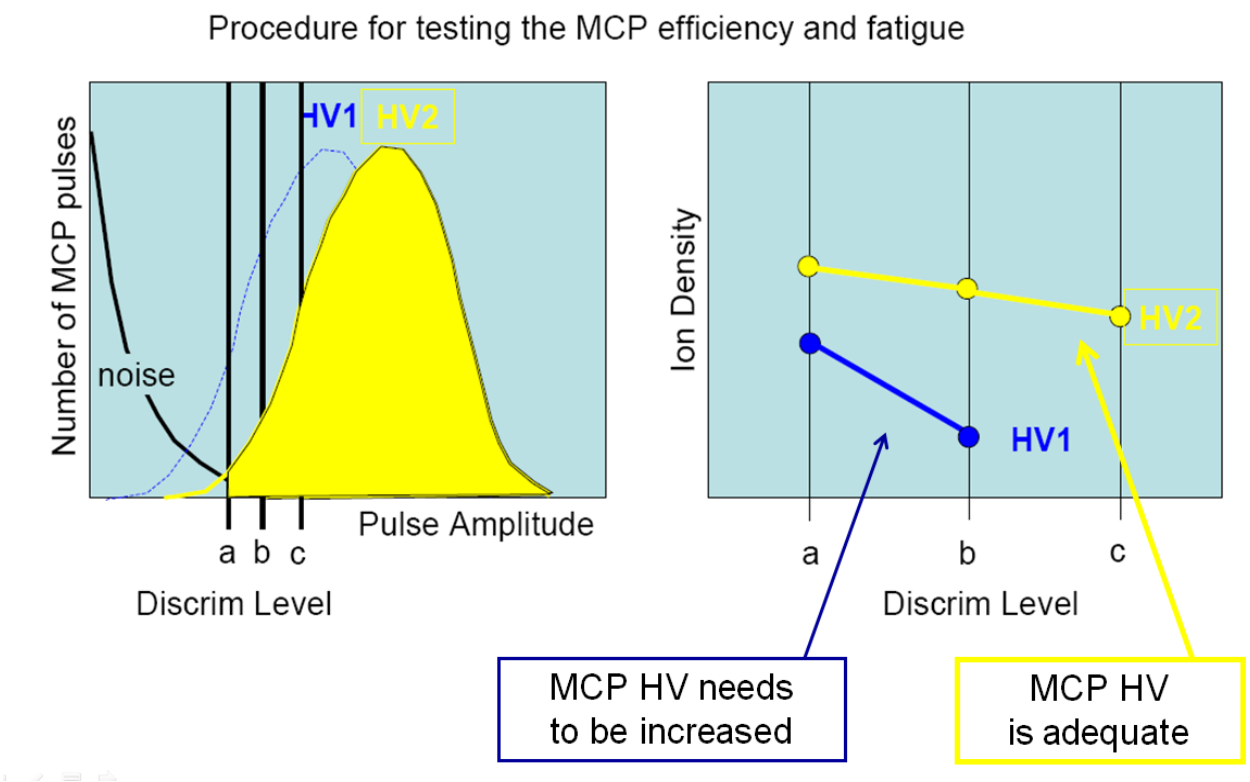

Figure 3.1

Onboard calibration principle:

Procedure for testing the MCP detection efficiency and fatigue. It involves testing combinations of MCP high-voltage levels and discriminator threshold levels.

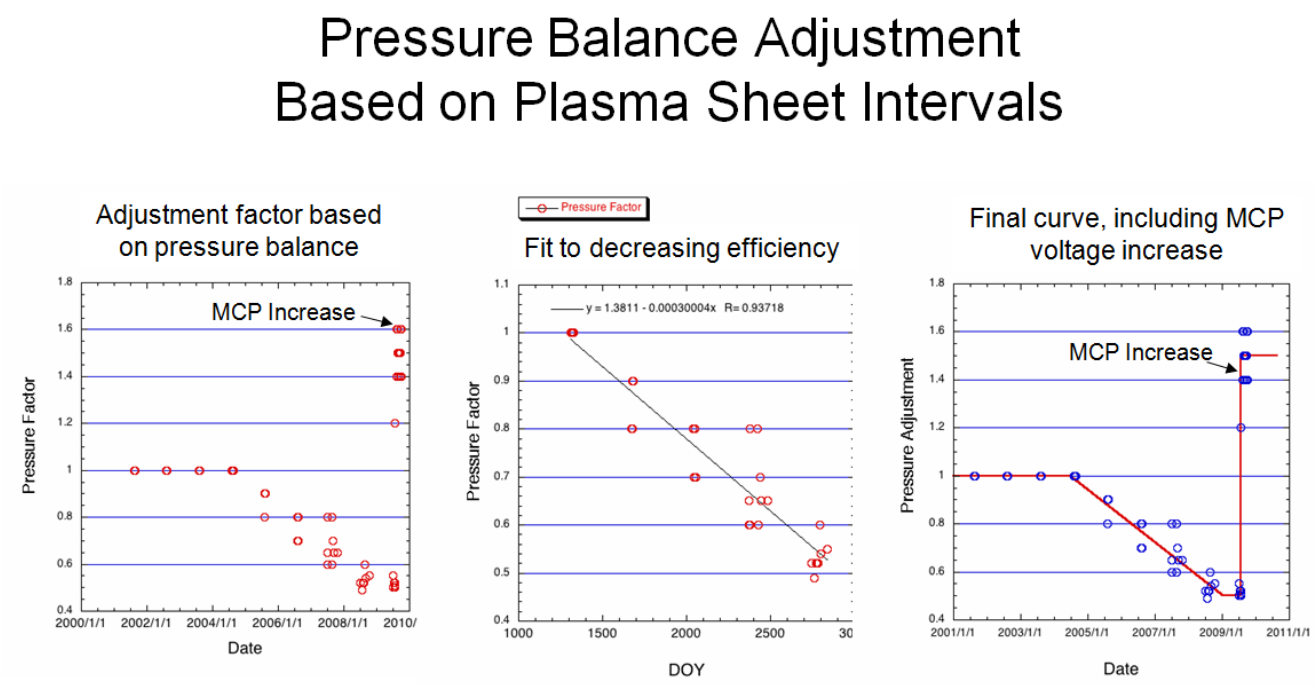

Figure 3.2

Pressure balance test (sum of ion and magnetic field pressure) used for estimating the CODIF efficiency change. It shows the derived pressure balance factor, the fit to the drop-off, and then the final curve. This adjustment is then applied to the current calibration curve.

The CODIF calibrations updating is a complex process. It involves :

- the determination of the start-MCP efficiency
- the stop-MCP efficiency
- the fraction of coincidences between the "start" and the "stop" signal that also have a single position signal, allowing thus to calculate the total efficiency
- In addition, the efficiencies of the individual anodes (for each 22.5° sector) have to be cross-calibrated
- calibrations involve also separate efficiencies determination for the four main ion species

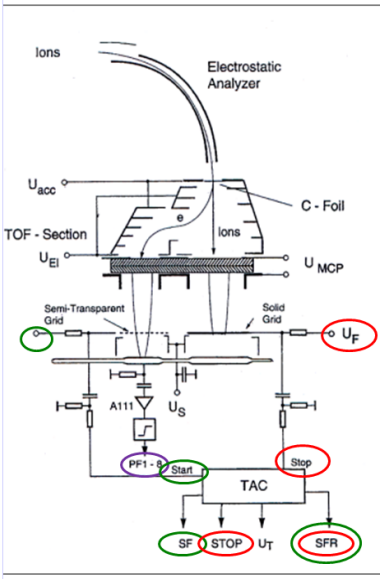

Figure 3.3

CODIF calibrations updating procedure. The main signals, provided by the ion time-of-flight system, are highlighted in the instrument schematic on the right.

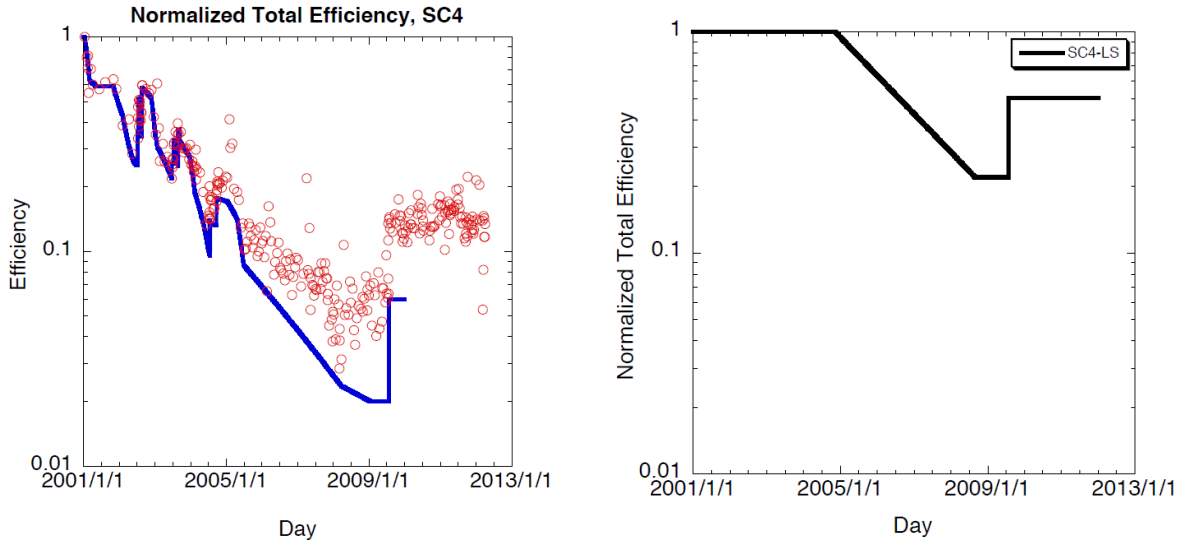

Figure 5.1

CODIF Cluster 4 H^+ efficiency evolution for the HS side (left) and for the LS side (right). Normalized total efficiencies derived using only rate data are shown in red circles, and after the adjustments based on the pressure balance technique are shown with the blue line. All efficiencies are normalized to 1.0 at the start of the mission. From Kistler et al., 2013.

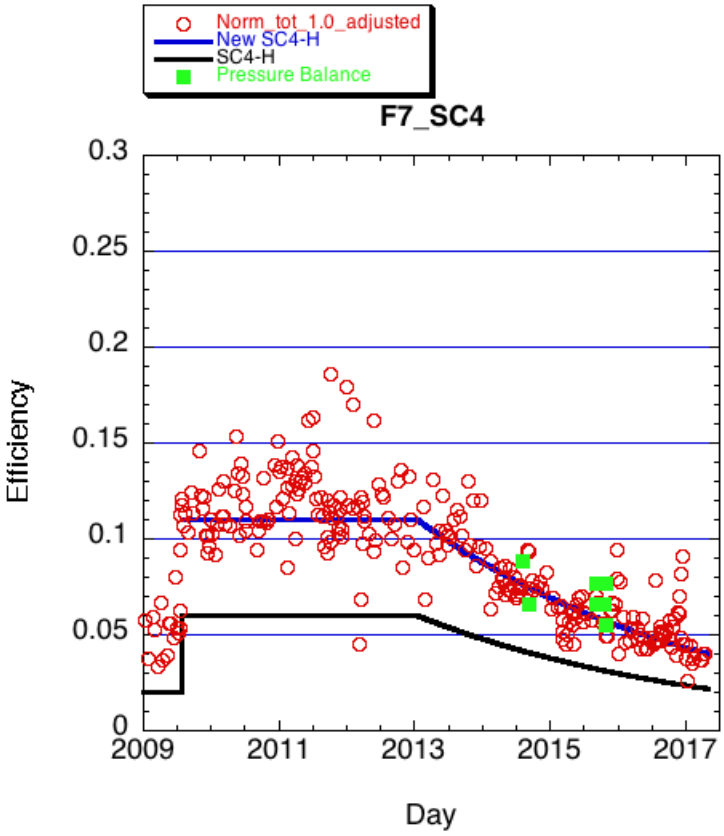

Figure 5.2.

CODIF Cluster 4 H^+ efficiency evolution for the HS side, following the 2009 MCP high-voltage raise. The blue curve represents the adopted efficiency values.

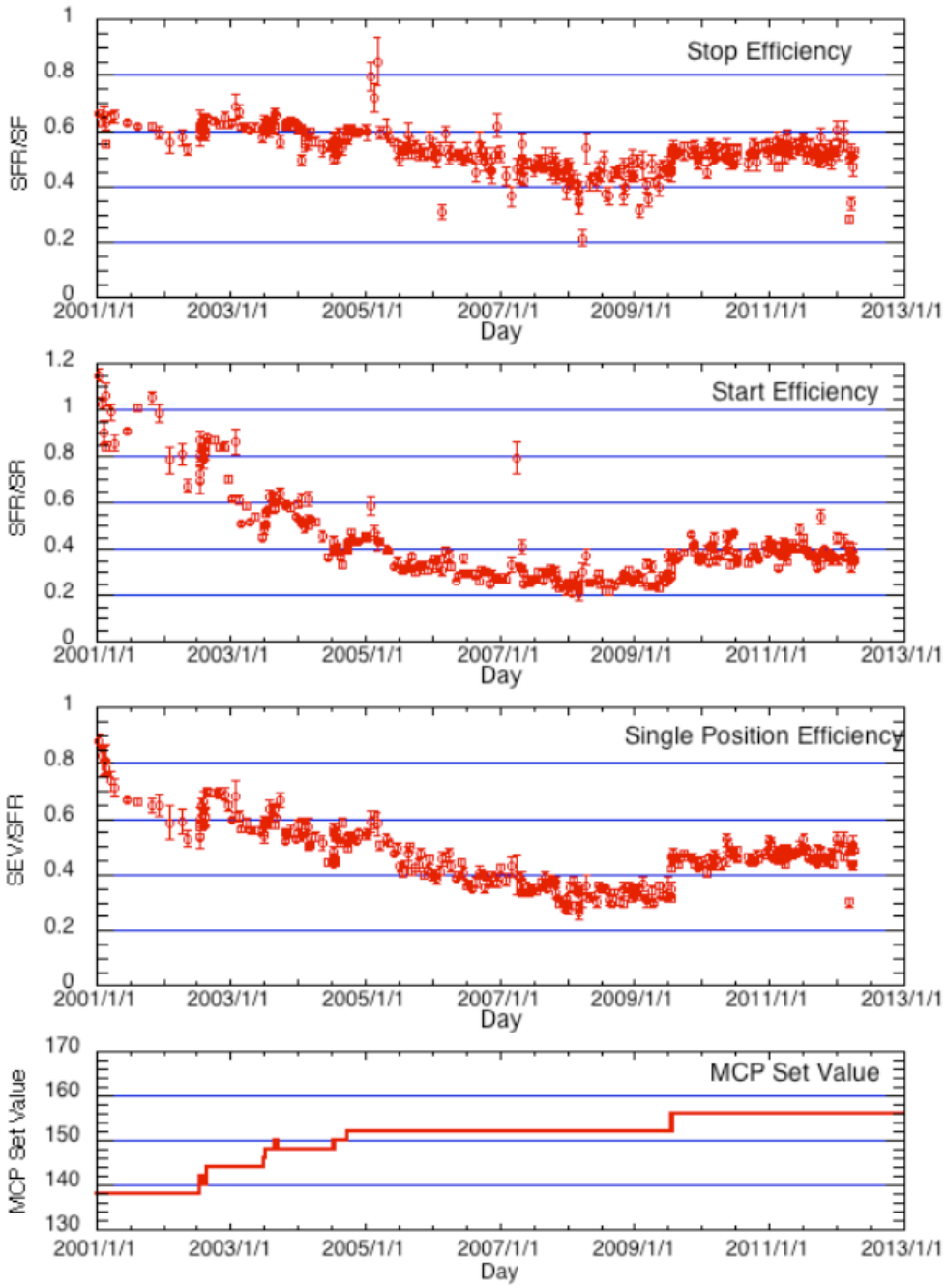

Figure 5.3

Cluster 4 CODIF efficiencies for 1 keV H^+ ions, for the "Stop", "Start" and "Single Position" signals. The evolution on the high-voltage value applied on the MCP, through the mission, is in the bottom panel.

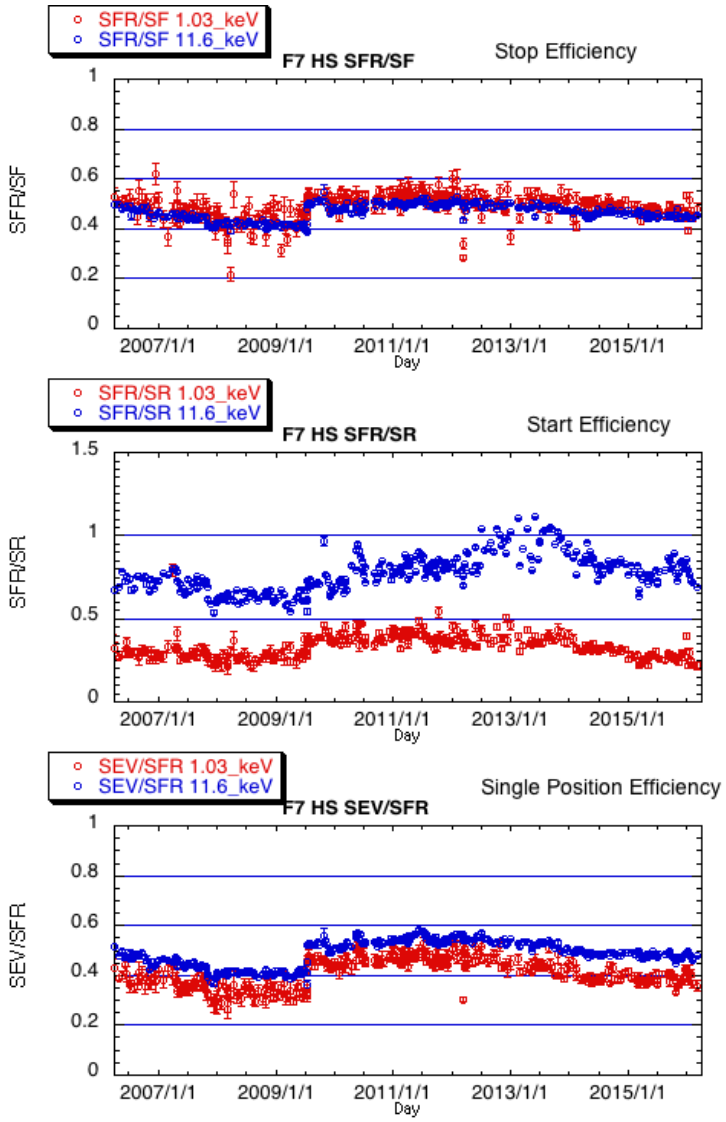

Figure 5.4

Cluster 4 CODIF efficiencies for 1.03 keV and for 11.6 keV H^+ ions, for the "Stop", "Start" and "Single Position" signals, for the period September 2006 to July 2015.

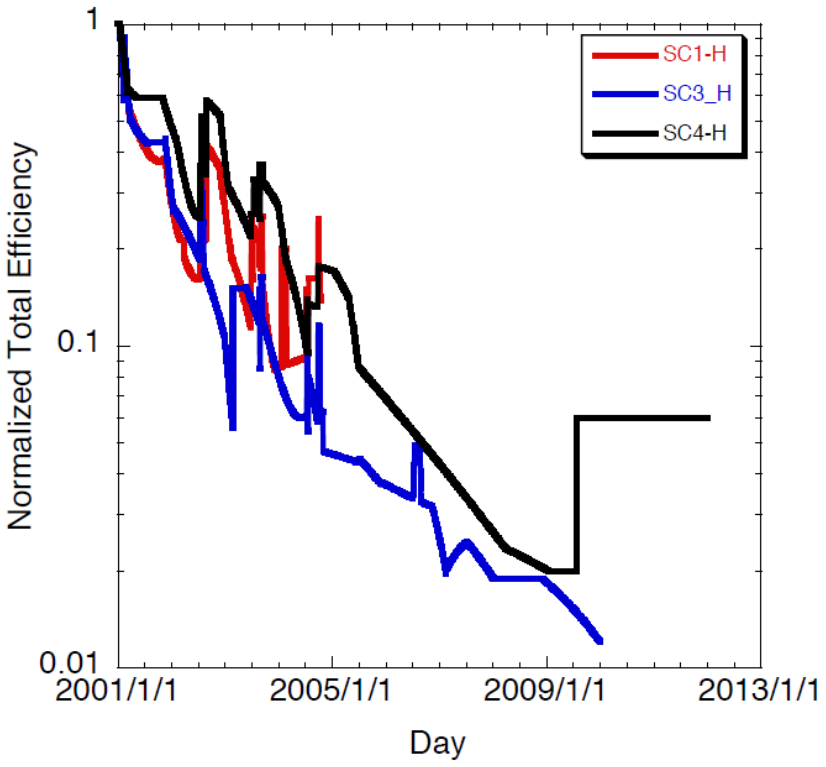

Figure 5.5

CODIF Cluster 1, 3 and 4 total H^+ efficiencies evolution, normalised to the start of the mission. From Kistler et al., 2013.

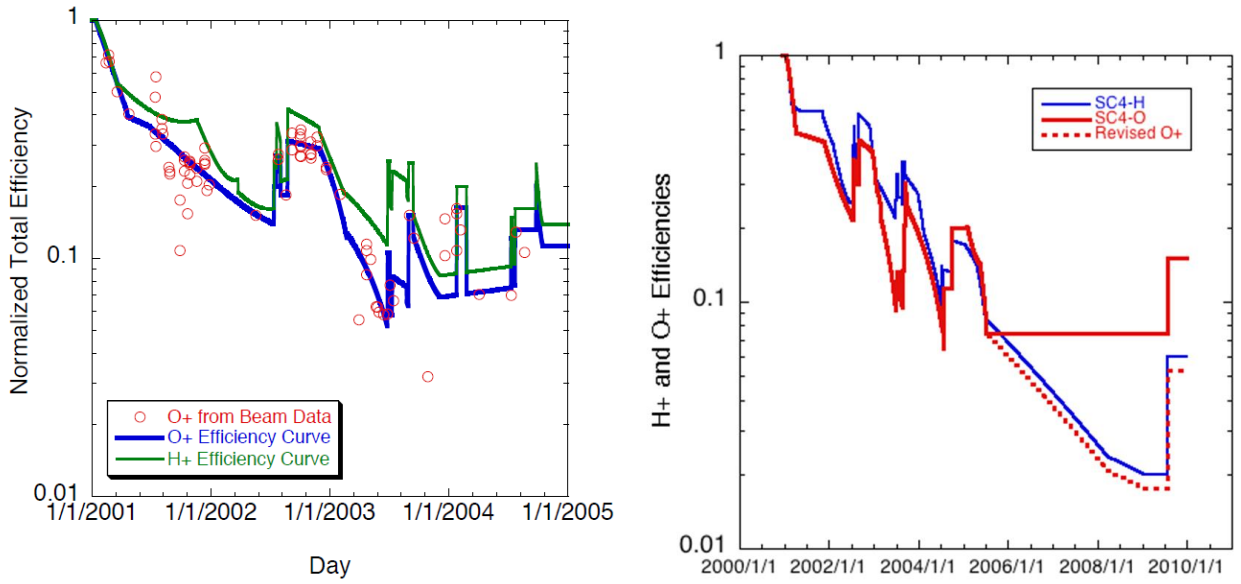

Figure 5.6

CODIF Cluster 1 (left) and Cluster 4 (right) O^+ efficiencies evolution, HS side.
Left: O^+ normalized total efficiency derived using the O^+ beam data for Cluster 1. The final curve used for the O^+ efficiency is shown with the blue line, and the H^+ efficiency is shown in green, for comparison.
Right: O^+ normalized total efficiency for Cluster 4 (in red). The dotted line shows the values revised in 2013, obtained from analyzing long-term trends (over a solar cycle) and evolution of the O^+/H^+ ratio. The H^+ efficiency is shown in blue, for comparison.

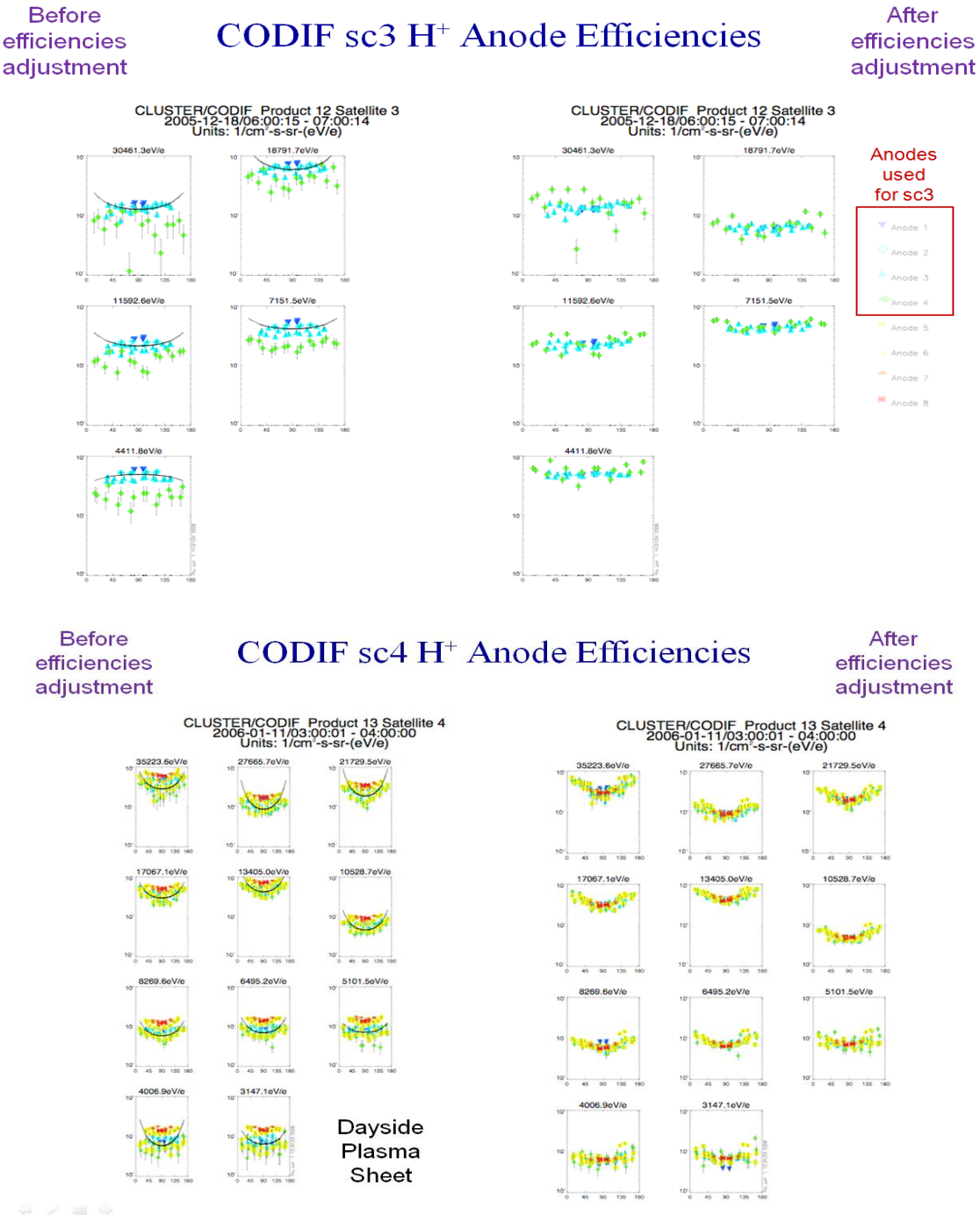

Figure 5.7

CODIF anodes cross-calibrations, in an isotropic plasma: before efficiencies adjustment (left), and after correcting for relative efficiencies (right). Plots are pitch-angle distributions for different energies, and colors correspond to the different anodes.

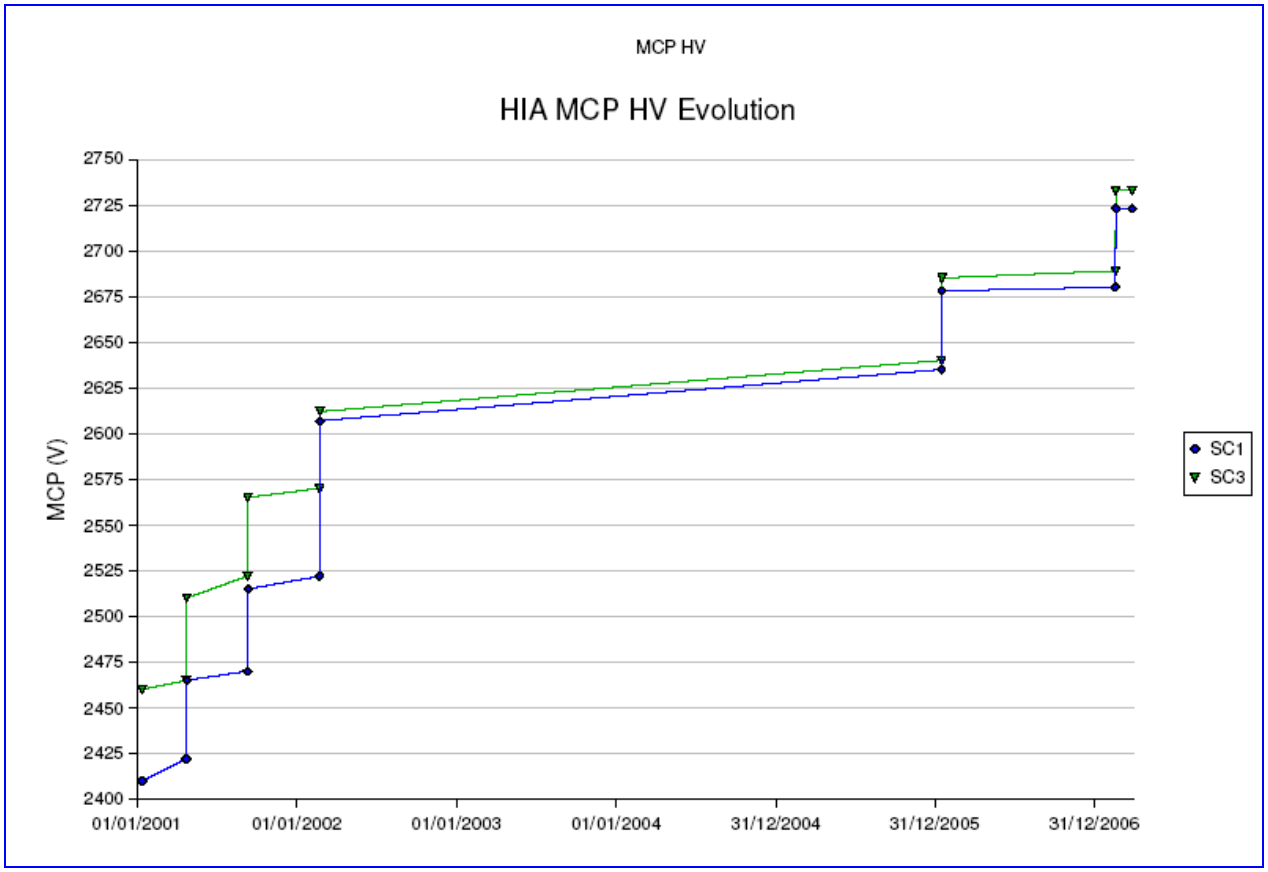

Figure 5.8

HIA MCP HV evolution for Cluster 1 (blue) and Cluster 3 (green).

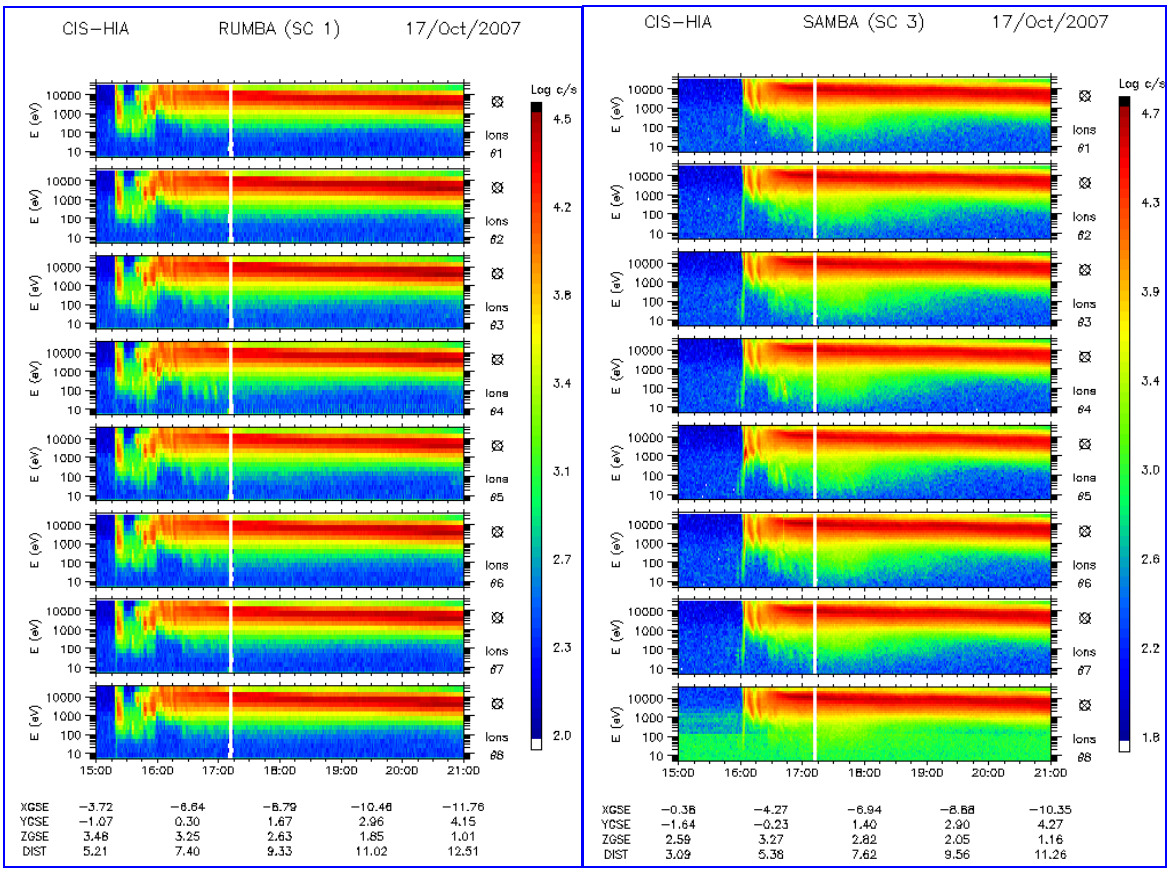

Figure 5.9

HIA MCP anode response in an isotropic plasma (corrected for relative anode efficiencies), for Cluster 1 and Cluster 3.

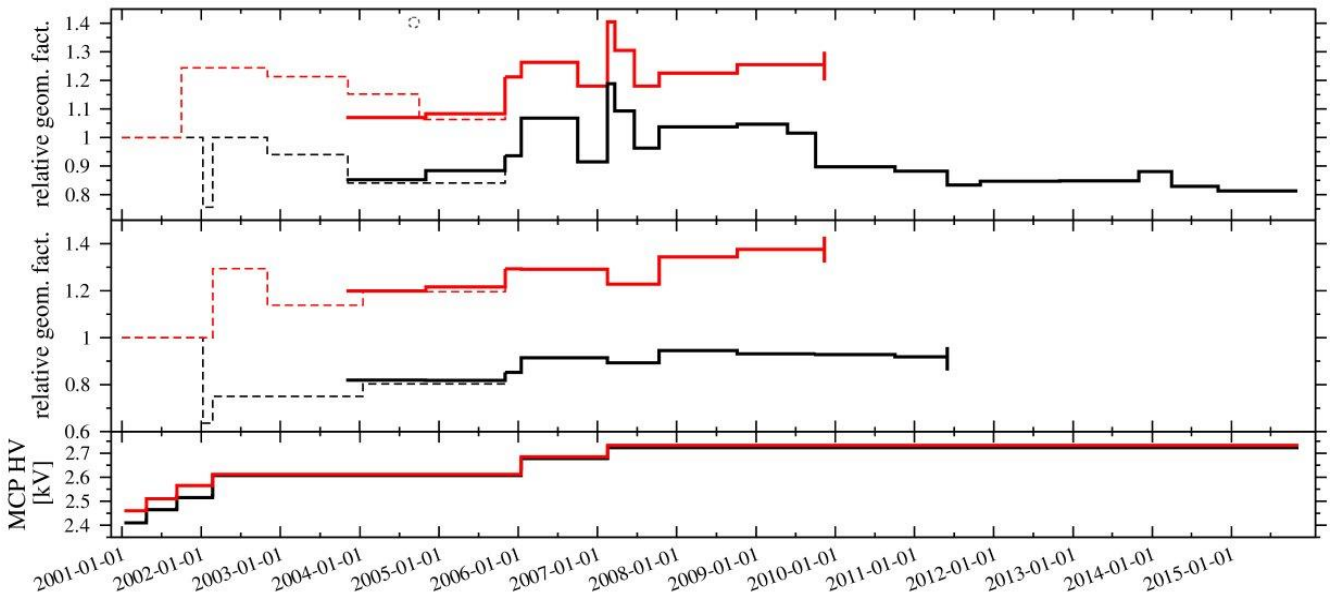

Figure 5.10

Evolution of the HIA calibration factors for Cluster 1 (black) and Cluster 3 (red): HS side (top panel) and LS-side (medium panel). Dashed lines are for in-flight calibrations performed early in the mission. The high-voltage values applied on the MCPs, through the mission, are shown for reference in the bottom panel.

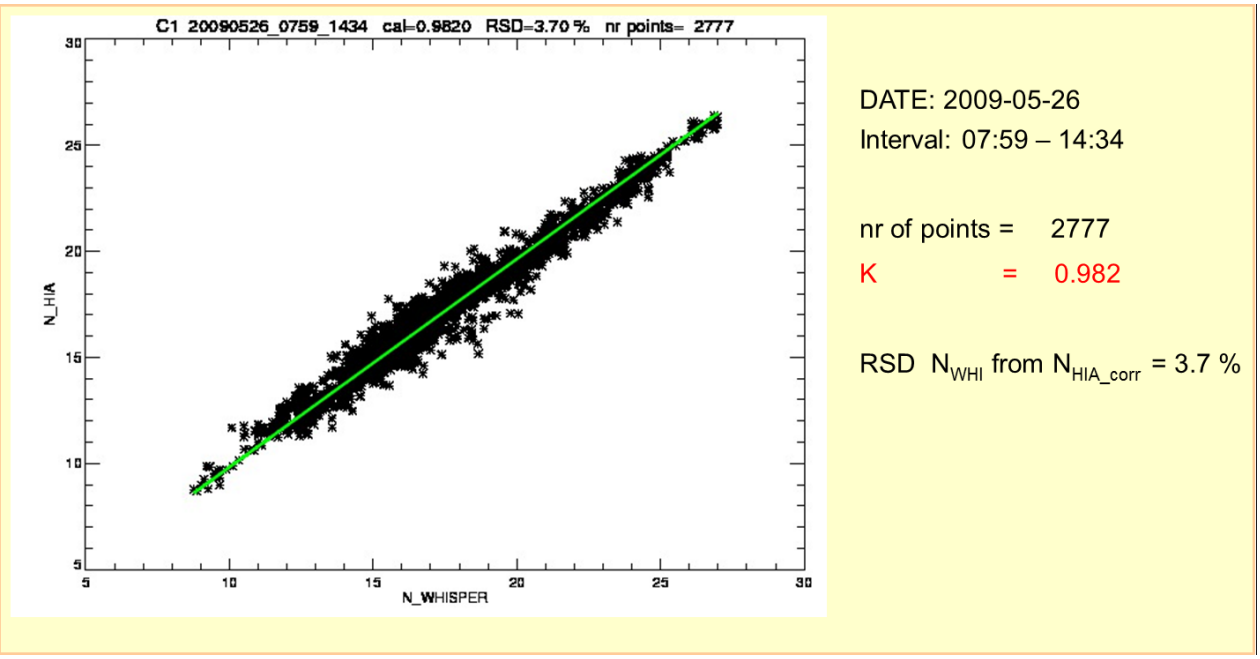

Figure 6.1

HIA - Whisper density cross-calibration in the magnetosheath.

Example of a 2009 event, used in fine-tuning HIA calibrations.

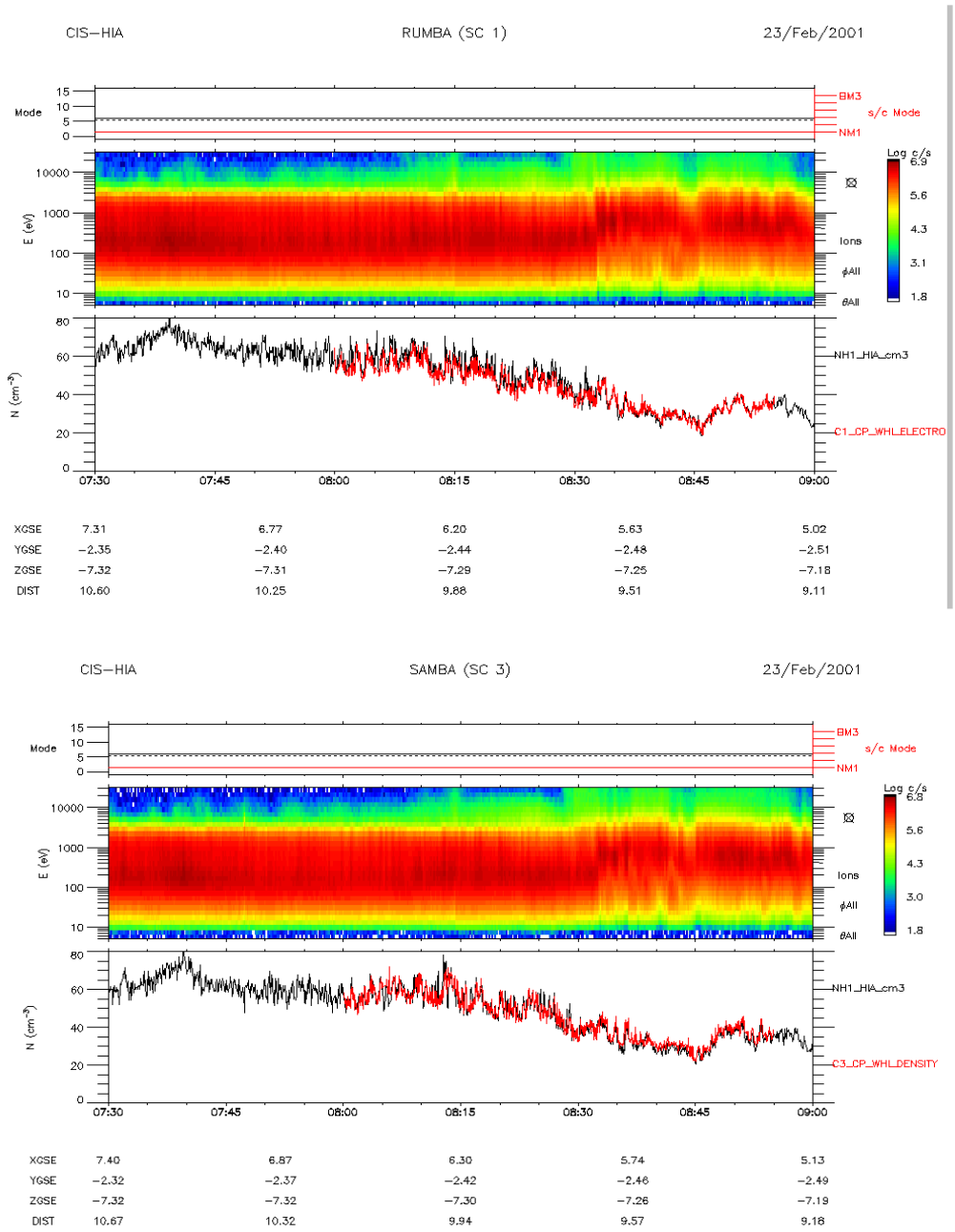

Figure 6.2

Typical HIA - WHISPER density cross-calibration results, in the magnetosheath. HIA density in black, and WHISPER provided density in red. WHISPER density data courtesy of the WHISPER team and the CAA.

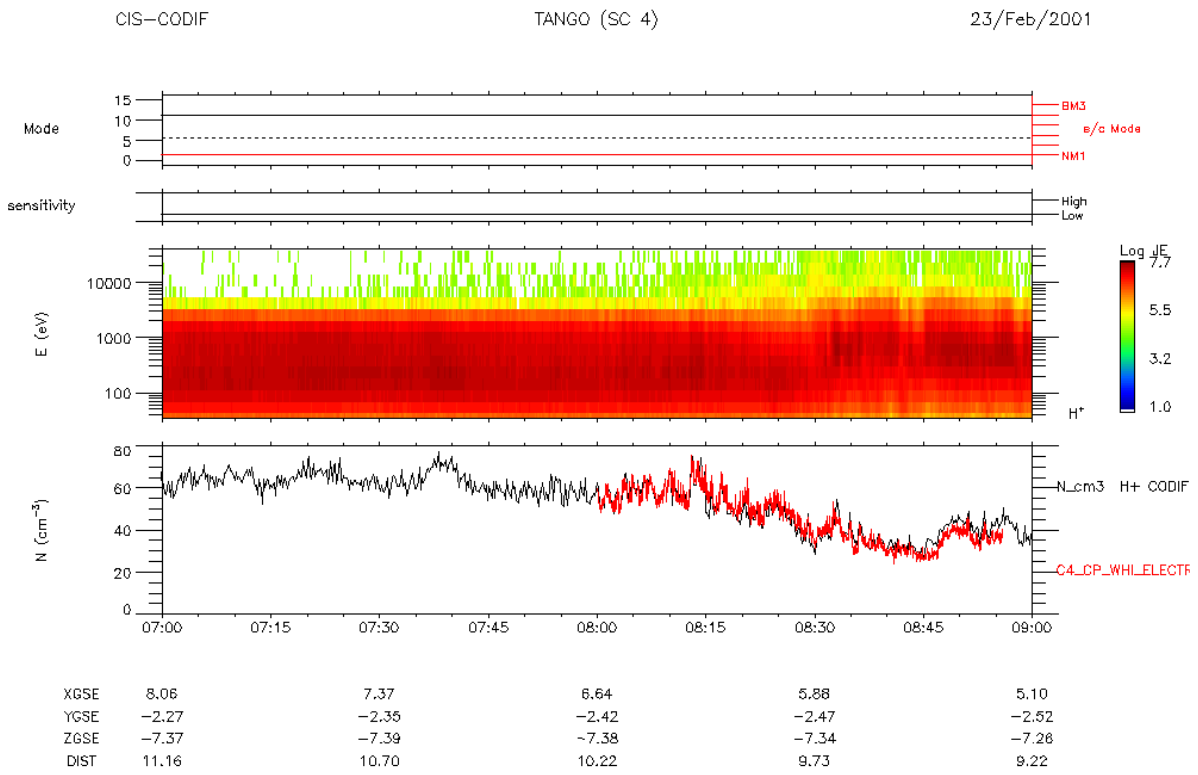

Figure 6.3

Typical CODIF (low-sensitivity side) - WHISPER density cross-calibration results, in the magnetosheath. CODIF density in black, and WHISPER provided density in red. WHISPER density data courtesy of the WHISPER team and the CAA.

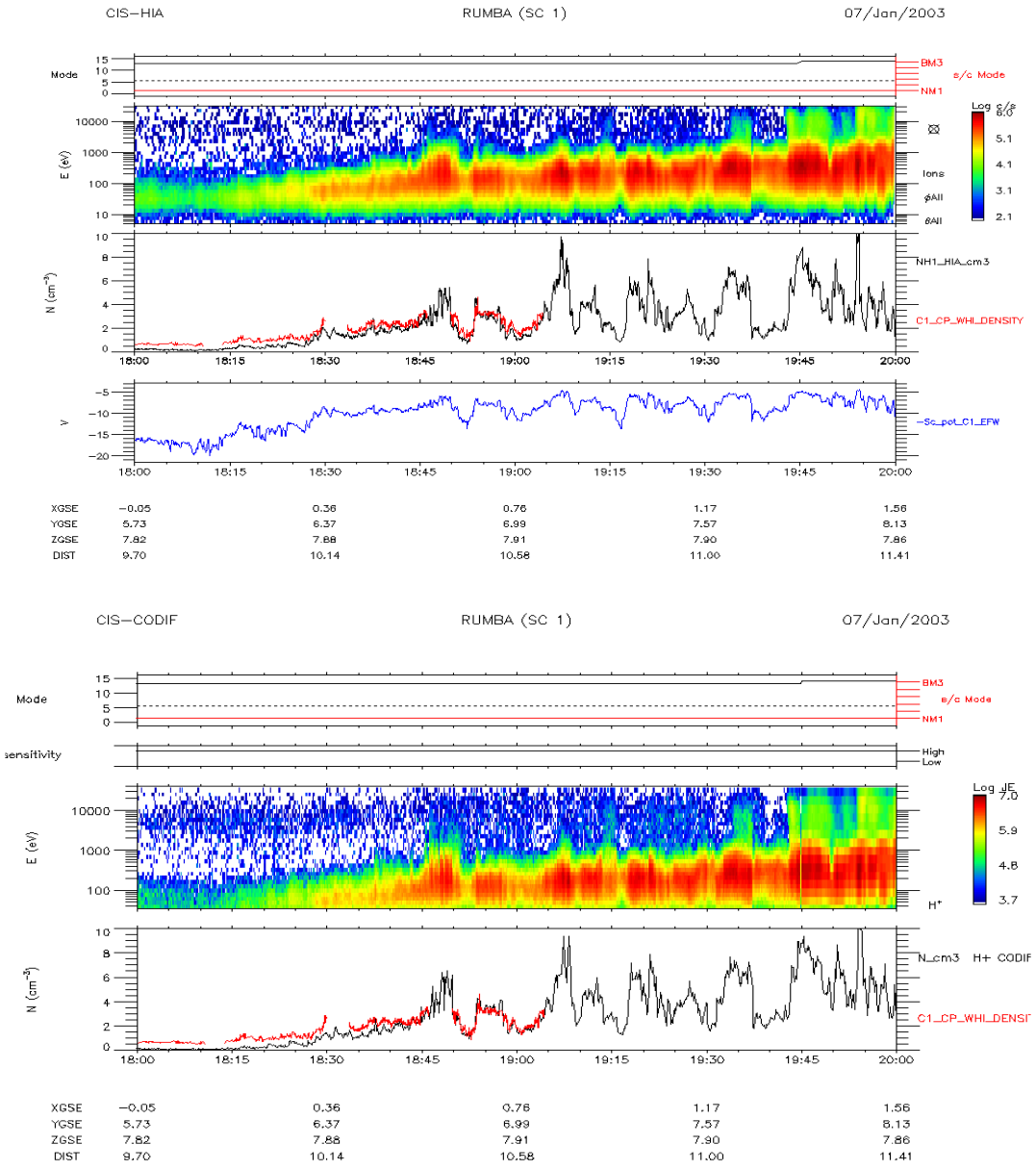

Figure 6.4

Typical HIA (top panels) and CODIF (bottom panels) - WHISPER density cross-calibration results, in the cusp. HIA and CODIF density plots in black (both instruments are operating in the high-sensitivity side), and WHISPER provided density plot in red. In blue is the negative of the spacecraft potential, measured by the EFW experiment. WHISPER data courtesy of the WHISPER team and the CAA. EFW data courtesy of the EFW team and the CAA.

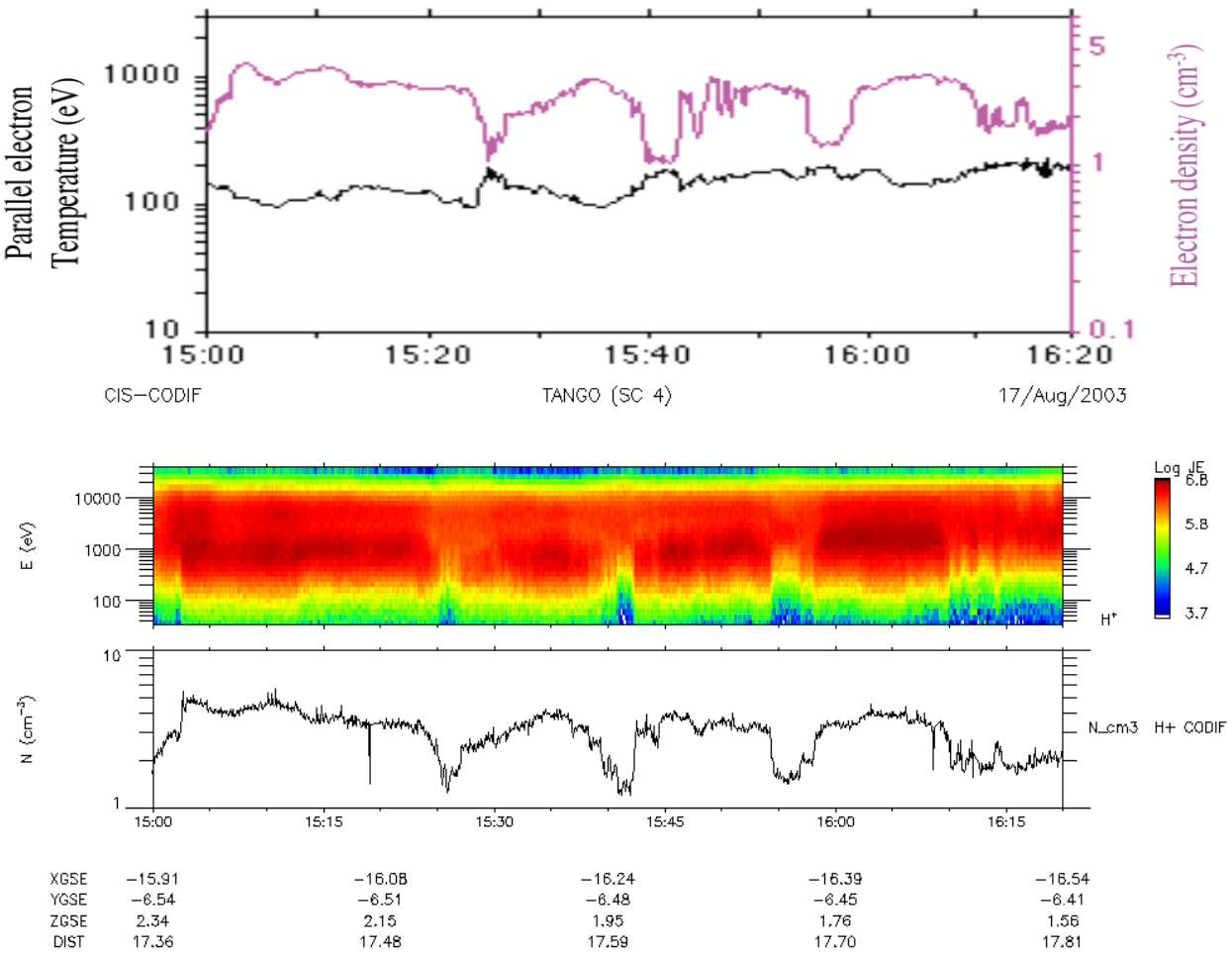

Figure 6.5

PEACE provided density (magenta curve, top panel) compared to CODIF (high-sensitivity side) density (bottom panel) in a dense plasma sheet. From Masson et al., (2010).

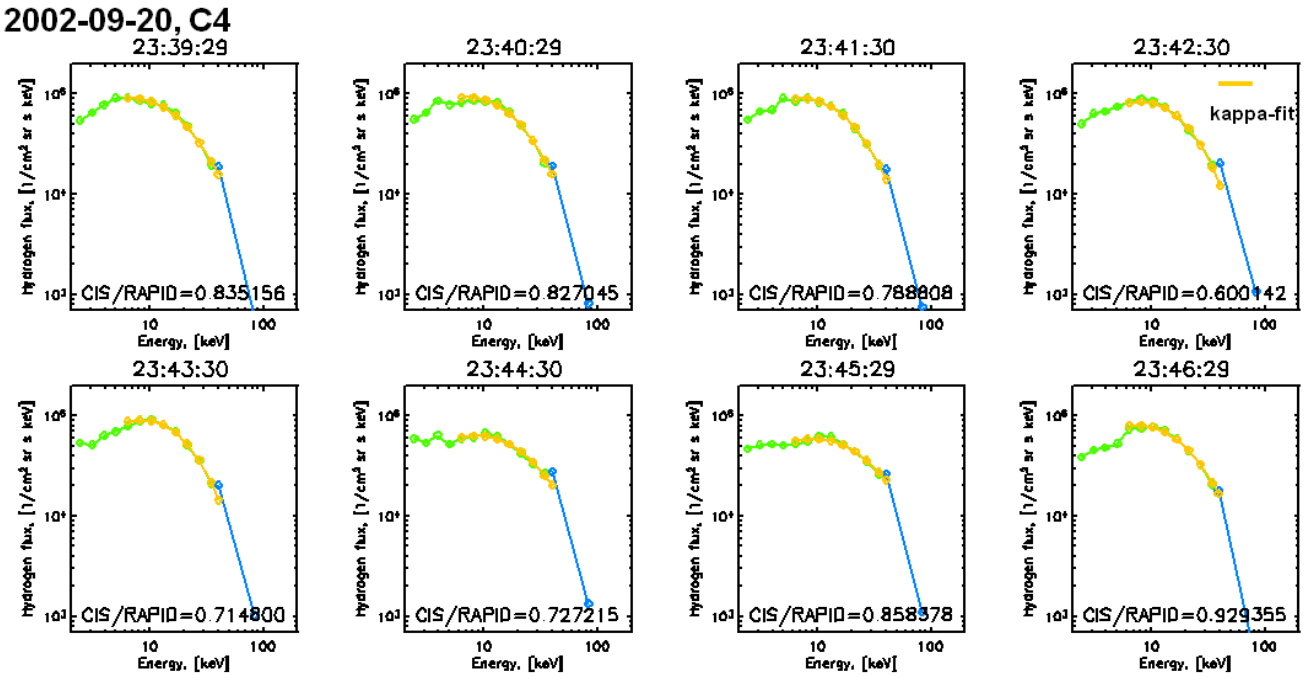

Figure 6.6

Example of composite ion energy spectra: CODIF (green), RAPID (blue), and kappa-fit (yellow), in the plasma sheet. cf. Kronberg et al., 2010.

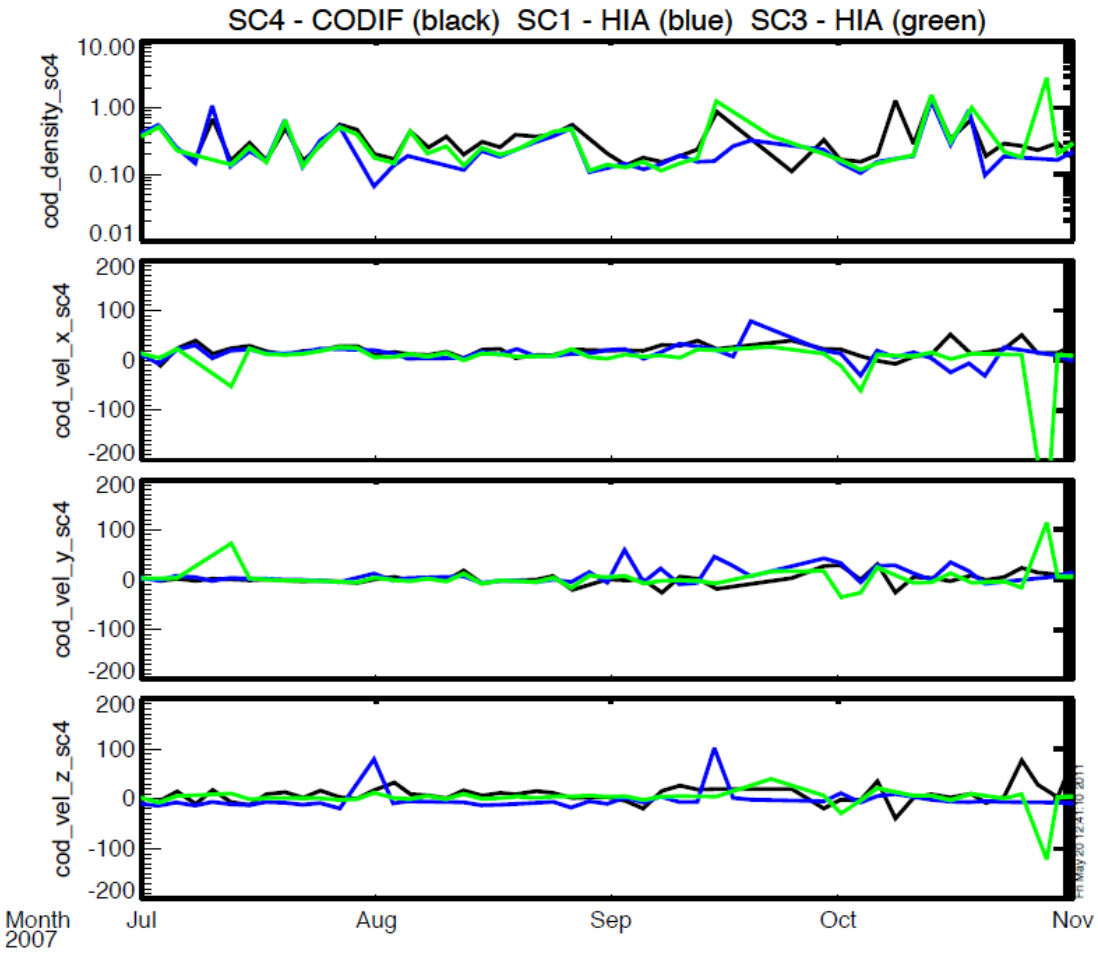

Figure 6.7

CODIF-HIA densities and velocities comparisons: average densities and velocities in the plasma sheet from CODIF, on Cluster 4, and from HIA on Cluster 1 and Cluster 3. cf. Kistler et al., 2013.